

1 **Expression of a CO₂-permeable aquaporin enhances mesophyll conductance in the C₄**
2 **species *Setaria viridis***

3 **Maria Ermakova^{1*}, Hannah Osborn¹, Michael Groszmann¹, Soumi Bala¹, Andrew Bowerman¹,**
4 **Samantha McGaughey¹, Caitlin Byrt¹, Hugo Alonso-Cantabrana¹, Steve Tyerman², Robert T.**
5 **Furbank¹, Robert E. Sharwood^{1,3*}, Susanne von Caemmerer¹**

6 ¹ Australian Research Council Centre of Excellence for Translational Photosynthesis, Division of Plant
7 Science, Research School of Biology, The Australian National University, Acton, Australian Capital
8 Territory, 2601, Australia

9 ² ARC Centre of Excellence in Plant Energy Biology, School of Agriculture Food and Wine, University of
10 Adelaide, Glen Osmond, South Australia, 5064, Australia

11 ³ Hawkesbury Institute for the Environment, Western Sydney University, Richmond, NSW, 2753,
12 Australia

13 ***Corresponding authors:** maria.ermakova@anu.edu.au and r.sharwood@westernsydney.edu.au

14 **Key words:** *Setaria viridis*, *Setaria italica*, aquaporin, CO₂ diffusion, mesophyll conductance, C₄
15 photosynthesis, C¹⁸O¹⁶O discrimination

16

17 **Abstract**

18 A fundamental limitation of photosynthetic carbon fixation is the availability of CO₂. In C₄ plants,
19 primary carboxylation occurs in mesophyll cytosol, and little is known about the role of CO₂ diffusion
20 in facilitating C₄ photosynthesis. We have examined the expression, localization, and functional role
21 of selected plasma membrane intrinsic aquaporins (PIPs) from *Setaria italica* (foxtail millet) and
22 discovered that *SiPIP2;7* is CO₂-permeable. When ectopically expressed in mesophyll cells of *S. viridis*
23 (green foxtail), *SiPIP2;7* was localized to the plasma membrane and caused no marked changes in leaf
24 biochemistry. Gas-exchange and C¹⁸O¹⁶O discrimination measurements revealed that targeted
25 expression of *SiPIP2;7* enhanced the conductance to CO₂ diffusion from the intercellular airspace to
26 the mesophyll cytosol. Our results demonstrate that mesophyll conductance limits C₄ photosynthesis
27 at low *p*CO₂ and that *SiPIP2;7* is a functional CO₂ permeable aquaporin that can improve CO₂ diffusion
28 at the airspace/mesophyll interface and enhance C₄ photosynthesis.

29

30 **Introduction**

31 Diffusion of CO₂ across biological membranes is a fundamental aspect to photosynthesis. The
32 significant contribution of aquaporins to increased CO₂ diffusion has been demonstrated in C₃ plants
33 (Flexas et al., 2006; Hanba et al., 2004; Sade et al., 2010). Aquaporins have key roles in regulating the
34 movement of water and solutes into roots and between tissues, cells and organelles (Tyerman,
35 McGaughey, Qiu, Yool, & Byrt, 2021). These pore-forming integral membrane proteins can be divided
36 into multiple sub-families depending on their amino acid sequence and sub-cellular localization. The
37 PIPs (p_lasma m_embrane i_ntrinsic p_roteins) are the only sub family, to date, known to permeate CO₂
38 (Uehlein, Kai, & Kaldenhoff, 2017). The PIPs are subdivided into paralog groups PIP1s and PIP2s,
39 based on sequence homology (Azad et al., 2016; Chaumont, Barrieu, Wojcik, Chrispeels, & Jung,
40 2001; Groszmann, Osborn, & Evans, 2017). Typically, PIP2s show higher water permeability when
41 expressed in heterologous systems (Chaumont, Barrieu, Jung, & Chrispeels, 2000) and PIP1s
42 seemingly require interaction with a PIP2 to correctly traffic to the plasma membrane (Berny, Gilis,
43 Rooman, & Chaumont, 2016; Zelazny et al., 2007). In plants, a number of CO₂ permeable PIPs have
44 been identified including *Arabidopsis thaliana* AtPIP1;2 (Heckwolf, Pater, Hanson, & Kaldenhoff,
45 2011) and AtPIP2;1 (Wang et al., 2016); *Hordeum vulgare* HvPIP2;1, HvPIP2;2, HvPIP2;3 and HvPIP2;5
46 (Mori et al., 2014); *Nicotiana tabacum* NtPIP1;5s (NtAQP1) (De Rosa, Watson-Lazowski, Evans, &

47 Groszmann, 2020; Uehlein, Lovisolo, Siefritz, & Kaldenhoff, 2003) and *Zea mays* ZmPIP1;5 and
48 ZmPIP1;6 (Heinen et al., 2014).

49 The roles of the CO₂ permeable aquaporins have been largely characterized in C₃ photosynthetic
50 plants where aquaporins localized in both the plasma membrane and the chloroplast envelope have
51 been shown to facilitate CO₂ diffusion from the intercellular airspace to the site of Rubisco in
52 chloroplasts (Kaldenhoff, 2012; Uehlein et al., 2008). The capacity for CO₂ diffusion to the initial sites
53 of carboxylation influences the amount of water loss through transpiration (Cousins, Mullendore, &
54 Sonawane, 2020). Therefore, by providing a more efficient pathway for CO₂ diffusion, these
55 membrane pores may contribute to increasing the water-use-efficiency (Groszmann et al., 2017).
56 However, little is known about the role of CO₂ permeable aquaporins and their influence on CO₂
57 diffusion from substomatal cavities to the first site of carboxylation in C₄ photosynthesis. The C₄
58 photosynthetic pathway is a biochemical CO₂ pump where the initial conversion of CO₂ to
59 bicarbonate (HCO₃⁻) by carbonic anhydrase (CA) and subsequent fixation of phosphoenolpyruvate
60 (PEP) by PEP carboxylase (PEPC) takes place in the cytosol of mesophyll cells. The pathway requires a
61 close collaboration between mesophyll and bundle sheath cells and this constrains leaf anatomy
62 limiting mesophyll surface area that forms a diffusive interface for CO₂ (Evans & von Caemmerer,
63 1996). Mesophyll conductance is defined as the conductance to CO₂ diffusion from the intercellular
64 airspace to the mesophyll cytosol (Evans & von Caemmerer, 1996; Osborn et al., 2016; Ubierna,
65 Gandin, Boyd, & Cousins, 2017). Although the rate of C₄ photosynthesis is almost saturated at
66 ambient *p*CO₂, current modelling suggests that higher mesophyll conductance can increase
67 assimilation rate and water-use-efficiency at low intercellular CO₂ partial pressures which occur when
68 stomatal conductance is low (von Caemmerer & Furbank, 2016).

69 *Setaria italica* (foxtail millet) and *Setaria viridis* (green foxtail) are C₄ grasses of the Paniceae tribe and
70 Poaceae family, related to important agronomical crops such as *Z. mays* (maize) and *Sorghum bicolor*
71 (sorghum). *S. viridis* is frequently used as a model species for C₄ photosynthesis research as it is
72 diploid with a relatively small genome that is sequenced and can be easily transformed (Brutnell et
73 al., 2010; Ermakova, Lopez-Calcano, Raines, Furbank, & von Caemmerer, 2019; Osborn et al., 2016).
74 Here we used a yeast heterologous expression system to examine the permeability to CO₂ of selected
75 PIPs from *S. italica*. We identified *SiPIP2;7* as encoding a CO₂-permeable aquaporin that, when
76 expressed in the plasma membrane of *S. viridis* mesophyll cells, increased mesophyll conductance.
77 Our results demonstrate that CO₂-permeable aquaporins can be used to increase CO₂ diffusion from
78 the intercellular airspace to mesophyll cytosol to provide higher carboxylation efficiency in C₄ leaves.

79

80 **Results**

81 ***S. italica* PIP family**

82 Four *PIP1* and eight *PIP2* genes were identified in both *S. italica* and *S. viridis* and their protein
83 sequences were 99–100 % identical between the two species (Supplementary File 1). Phylogenetic
84 analysis based on the amino acid sequences of the *S. italica* PIP family showed that three distinct
85 clades emerge: the *PIP1* clade, *PIP2* clade I, and *PIP2* clade II (Figure 1-figure supplement 1). Isoforms
86 within these three clades have characteristic differences including sequence signatures associated
87 with substrate selectivity (Supplementary File 2). Three of *SiPIP1*s (1;1, 1;2, 1;5) and all *SiPIP2* clade I
88 members (2;1, 2;4, 2;5, 2;6, 2;7) matched the current consensus sequence for CO₂ transport (Azad et
89 al., 2016; Perez Di Giorgio et al., 2014).

90 RNA-seq data from the publicly available Phytomine database (Phytozome), was examined for tissue-
91 specific expression patterns of the *S. italica* *PIPs* (Figure 1a). *SiPIP1*;1, 1;2, 1;5, and 2;1 express at
92 moderate to high levels and *SiPIP2*;6 at low to moderate levels, in all tissues analyzed (root, leaves,
93 shoot, panicle). *SiPIP1*;6, 2;4, 2;5, 2;7 and 2;3 were expressed predominantly in roots at low to
94 moderate levels. *SiPIP2*;8 was expressed only in leaves and *SiPIP2*;2 transcripts were not detected.

95 **Functional characterization of PIPs**

96 GFP localization of *SiPIP*-GFP fusions were used to confirm expression and determine targeting to the
97 yeast plasma membrane (Figure 1b). Overall, *SiPIP1*s had lower GFP signal that was patchy at the cell
98 periphery with strong internal signal consistent with localization to the endoplasmic reticulum. GFP
99 signal was also present diffusively throughout the cytosol suggestive of protein degradation. Overall,
100 *SiPIP1*s were poorly produced in yeast and were not efficiently targeting to the plasma membrane as
101 needed for the functional assays. For the *PIP2*s, only *SiPIP2*;1, *SiPIP2*;4, *SiPIP2*;5, and *SiPIP2*;7 showed
102 clear localization to the plasma membrane in addition to other internal structures, and were
103 therefore selected for further functional analyses.

104 CO₂ permeability was measured in yeast co-expressing a *SiPIP* along with *human CARBONIC*
105 *ANHYDRASE II (hCAII)*. A stopped flow spectrophotometer was used to monitor CO₂-triggered
106 intracellular acidification via changes in fluorescence intensity of a pH sensitive fluorescein dye
107 (Figure 1-figure supplement 2) (Ding et al., 2013; Heckwolf et al., 2011; Uehlein et al., 2008).
108 Importantly for reliable results, all *SiPIP* yeast lines tested showed similar cell volumes and were not

109 limited by CA activity (Figure 1-figure supplement 2). A screen of the lines revealed that yeast
110 expressing *SiPIP2;7* had the highest CO₂ permeability of $1.5 \times 10^{-4} \text{ m s}^{-1}$, which was significantly larger
111 than the negative control expressing *hCAII* only (Figure 1c). Other *SiPIPs* displayed comparable CO₂
112 permeability to the *hCAII* only control. The changes in CO₂ permeability detected on the stopped flow
113 spectrophotometer for yeast expressing *SiPIP2;7* were not an artifact brought on by an increased
114 permeability to protons causing the intracellular acidification (Figure 1-figure supplement 3).

115 Freeze-thaw survival assays, which quantify water permeability of aquaporins (Tanghe et al., 2002),
116 provided further confirmation that the *SiPIPs* expressed in yeast were functional. Overexpression of
117 water permeable aquaporins greatly improves freeze-thaw tolerance in yeast, especially in the highly
118 compromised aquaporin knockout mutant *aqp1/2* (Tanghe et al., 2002). Yeast expressing the β -
119 glucuronidase reporter gene (515.GUS) was used as a control to show that the single freeze-thaw
120 treatment was effective in almost killing off the entire yeast population (Figure 1d). Consistent with
121 the poor plasma membrane localization and abundance of *SiPIP2;1*-GFP (Figure 1b), yeast expressing
122 *SiPIP2;1* did not show any protection to freeze-thaw treatments (Figure 1c). On the other hand,
123 *SiPIP2;4*, *2;5* and *2;7* all showed some level of protection, indicating that they permeated water and
124 were functional within the plasma membrane of yeast cells. For detailed characterisation of water
125 permeability, *SiPIP2;7* was expressed in *Xenopus laevis* oocytes. Swelling assay confirmed that
126 *SiPIP2;7* is a functional water channel (Figure 1-figure supplement 4).

127 **Expression of PIP2;7 in mesophyll cells of *S. viridis***

128 To confirm and exploit the CO₂ permeability characteristic of *SiPIP2;7* *in planta*, we created
129 transgenic *S. viridis* plants expressing *SiPIP2;7* with a C-terminal FLAG-tag fusion and under the
130 control of the mesophyll-preferential *Z. mays* PEPC promoter (Gupta et al., 2020; Salesse-Smith et al.,
131 2018). Out of 52 T₀ plants analyzed for *SiPIP2;7*-FLAG protein abundance and the hygromycin
132 phosphotransferase (*hpt*) gene copy number (Figure 2-figure supplement 1), lines 27, 44 and 52 were
133 selected for further analysis because they had the strongest FLAG signal per transgene insertion
134 number. Immunodetection of FLAG and photosynthetic proteins was performed on leaves of
135 homozygous transgenic plants (Figure 2a); azygous plants of line 44 were used as control hereafter.
136 Monomeric and dimeric *SiPIP2;7*-FLAG was detected in all transgenic plants (Figure 2-figure
137 supplement 1) and abundance of the prevalent dimeric form was used for relative quantification of
138 *SiPIP2;7* abundance (Figure 2a). Plants of line 44 had the highest production of *SiPIP2;7*-FLAG whilst
139 plants of lines 27 and 52 accumulated about 2-4 times less of this protein. Immunodetection of FLAG

on leaf cross-sections, visualized with confocal microscopy, confirmed partial localization of SiPIP2;7-FLAG to the plasma membrane of mesophyll cells (Figure 2c). Transcript analysis confirmed highly elevated expression of *SiPIP2;7-FLAG* in leaves, but not in roots of transgenic lines (Figure 2-figure supplement 2).

Abundances of photosynthetic proteins PEPC, CA, the Rieske subunit of the Cytochrome *b₆f* complex, and the small subunit of Rubisco (RbcS), did not differ between transgenic and control plants (Figure 2a). In line with the immunoblotting results, measured activities of PEPC and CA, and the amount of Rubisco active sites were not altered in the transgenic plants (Table 1). Chlorophyll content, leaf dry weight per area and biomass of roots and shoots did not differ between the genotypes either (Table 1).

To study the impact of *SiPIP2;7-FLAG* expression on the photosynthetic properties in transgenic plants, we conducted concurrent gas-exchange and chlorophyll fluorescence analyses at different intercellular CO₂ partial pressures (C_i) (Figure 3). No significant changes were detected between transgenic and control plants in CO₂ assimilation rates (A), effective quantum yield of Photosystem II (ϕ PSII) or stomatal conductance to water vapor at ambient CO₂ (Figure 3-figure supplement 1). The SiPIP2;7-FLAG protein abundance was compared to the gas-exchange phenotype in individual plants (Figure 3-figure supplement 2). A statistically significant polynomial relationship ($R^2 = 0.345$, $p < 0.05$) was found between the initial slopes and the relative protein content, which was significantly better than that achieved using a linear model ($p < 0.05$). No significant relationship was observed between the SiPIP2;7-FLAG abundance and the saturating rates of assimilation (A_{max} ; Figure 3-figure supplement 2).

Mesophyll conductance to CO₂ in plants expressing SiPIP2;7

Next, we analyzed in detail the initial slopes of the AC_i curves and mesophyll conductance. Fitting linear regressions indicated that mean \pm SE values of the initial slopes of the AC_i curves for lines 27, 44 and 52 were 0.46 ± 0.03 , 0.52 ± 0.01 and 0.53 ± 0.05 , respectively, compared to the value of 0.41 ± 0.02 in control plants (Figure 4a). Measurements of $\Delta^{18}O$ were used to estimate conductance of CO₂ from the intercellular airspace to the sites of CO₂ and H₂O exchange in the mesophyll cytosol (g_m) with the assumption that CO₂ was in full isotopic equilibrium with leaf water in the cytosol (Barbour, Evans, Simonin, & von Caemmerer, 2016; Osborn et al., 2016). Transgenic lines showed mesophyll conductance of 0.59 ± 0.05 , 0.55 ± 0.08 and 0.46 ± 0.04 mol m⁻² s⁻¹ bar⁻¹ compared to the mean \pm SE

value of $0.42 \pm 0.03 \text{ mol m}^{-2} \text{ s}^{-1} \text{ bar}^{-1}$ in control plants (Figure 4b). Two-way ANOVA analysis with Tukey post-hoc test on the initial slopes of the A/C_i curves and g_m showed that differences measured in plants of lines 27 and 44 were statistically significant from the control plants ($p = 0.04573$ and 0.03724 , respectively). Interestingly, for plants of line 52, only initial slopes were significantly different compared to control plants when compared by one-way ANOVA (Tukey post-hoc test, $\alpha = 0.05$, $p = 0.02993$).

We also used the g_m calculations proposed by Ogée, Wingate, and Genty (2018) which try to account for the rates of bicarbonate consumption by CA. The CA hydration constant (k_{CA}) of $6.5 \text{ mol m}^{-2} \text{ s}^{-1} \text{ bar}^{-1}$ was used for these calculations (Table 1). We found that the g_m measured with this method gave on average 1.25 times greater values but did not change the ranking of mesophyll conductance shown in Figure 4a (Figure 4-figure supplement 1). The C_4 photosynthetic model by von Caemmerer and Furbank (1999) and von Caemmerer (2000) relates the initial slope of the CO_2 response curve (dA/C_i) to g_m (see Figure 4 caption and Materials and Methods). Figure 4c shows that the measured relationship between the initial slope and g_m fits closely with model prediction.

Discussion

The diffusion of CO_2 from the earth's atmosphere to the site of primary carboxylation within leaves of C_3 and C_4 plants often limits photosynthesis and impacts the efficient use of water. Overexpression of CO_2 permeable aquaporins with the aim to enhance leaf CO_2 diffusion has been extensively probed in C_3 plants. Many studies have demonstrated that it was an effective strategy to improve g_m , leading to increased assimilation rate or grain yield (Flexas et al., 2006; Hanba et al., 2004; Uehlein et al., 2003; Xu et al., 2019). However, some published research could not identify a functional link between the CO_2 permeable aquaporins and mesophyll conductance, and possible explanations include functional redundancy between aquaporin isoforms (Kromdijk, Głowacka, & Long, 2020) and complications of expressing membrane proteins in the chloroplast envelope (Fernández-San Millán et al., 2018). In contrast to C_3 plants, where CO_2 needs to cross both plasma membrane and the chloroplast envelope to reach the site of carboxylation, the primary carboxylation step in C_4 plants occurs in the cytosol of mesophyll cells. Due to high photosynthetic rates of C_4 plants, this generates a large CO_2 drawdown between the intercellular airspaces and the cytosol and thus a large mesophyll conductance (Evans & von Caemmerer, 1996). Because only one membrane needs to be traversed by CO_2 , C_4 plants could serve as a simpler model to demonstrate the effect of CO_2 permeable aquaporins on photosynthesis.

200 Screening *S. italica* PIPs for CO₂ permeability in a yeast heterologous system resulted in identification
201 of SiPIP2;7 as a CO₂ pore (Figure 1c). Expression analysis revealed that *SiPIP2;7* was almost exclusively
202 expressed in roots under ideal conditions (Figure 1a, Figure 2-figure supplement 2) which, combined
203 with the water permeability identified in yeast and oocyte assays (Figure 1d, Figure 1-figure
204 supplement 4), suggest that SiPIP2;7 may function in regulating root hydraulic conductivity, a role
205 extensively documented for PIP aquaporins (Gambetta, Knipfer, Fricke, & McElrone, 2017;
206 McGaughey, Qiu, Tyerman, & Byrt, 2018). The physiological relevance of SiPIP2;7's CO₂ permeating
207 capacity is not immediately clear. Gas uptake by roots is well documented (Stemmet, De Bruyn, &
208 Zeeman, 1962) and in C₃ plants CO₂ uptake by roots may contribute to the C₄ photosynthesis-like
209 metabolism detected in stems and petioles (Hibberd & Quick, 2002). It is possible that *SiPIP2;7* is
210 conditionally expressed in leaves, or even that its capacity to transport CO₂ is inadvertent and related
211 to the transportation of another yet undetermined substrate; analogous to the uptake of toxic
212 metalloids by some NIP aquaporins due to their capacity to transport boron (Mukhopadhyay,
213 Bhattacharjee, & Rosen, 2014). Further work is needed to determine whether PIPs in general function
214 natively as relevant CO₂ pores in C₄ leaves.

215 We employed the CO₂ transport capacity of SiPIP2;7 to enhance transmembrane CO₂ diffusion from
216 the intercellular airspace into the mesophyll cytosol, where CA and PEPC reside, by overexpressing
217 *SiPIP2;7* in *S. viridis*. We confirmed the localization of SiPIP2;7 within the mesophyll plasma
218 membranes (Figure 2c) and detected the increase in CO₂ diffusion across the mesophyll membranes
219 in transgenic plants by two independent methods. First, we calculated g_m from the C¹⁸O¹⁶O
220 discrimination measurements (Figure 4b) and the theory for these calculations has been outlined
221 (Barbour et al., 2016; Ogée et al., 2018; Osborn et al., 2016). Second, we fitted linear regressions to
222 the initial slopes of the AC_i curves (Figure 4a), which depend on g_m , V_{pmax} and K_p where the two latter
223 parameters denote the maximum PEPC activity and the Michaelis Menten constant of PEPC for HCO₃⁻
224 (von Caemmerer, 2000; von Caemmerer & Furbank, 1999). Since PEPC and CA activities were not
225 altered in plants expressing *SiPIP2;7* (Table 1), higher initial slopes of the AC_i curves in transgenic lines
226 were attributed to the increased g_m . When plotted against each other, the initial slopes and g_m in
227 transgenic and control plants, fitted the model predictions confirming the hypothesised functional
228 role of g_m in C₄ photosynthesis (Pfeffer & Peisker, 1995; Ubierna et al., 2017; von Caemmerer, 2000).
229 Importantly, and in line with the model predictions, expression of SiPIP2;7 had an effect only on the
230 initial slopes of the AC_i curves but not on the saturating rates of assimilation (Figure 3-figure
231 supplement 2).

Our findings demonstrate that CO₂ permeable aquaporins can enhance CO₂ diffusion at the airspace/mesophyll interface in C₄ plants. However, overexpression of aquaporins is likely accompanied by confounding factors which could explain the lack of phenotype observed from the plants with the highest SiPIP2;7 expression level (Figure 3-figure supplement 2) and plants of line 52 showing significant increase of only initial slopes (Figure 4). These factors possibly include the transport of multiple substrate(s) by SiPIP2;7 and different efficiency of SiPIP2;7 targeting to the plasma membrane between the individual lines, plants, leaves and even between different mesophyll cells. Moreover, it is still not clear whether there are other CO₂-permeable aquaporins present in *S. viridis* leaves that account for the basal g_m level of $0.42 \pm 0.03 \text{ mol m}^{-2} \text{ s}^{-1} \text{ bar}^{-1}$ in control plants. Further research is required to unravel the aforementioned confounding factors. Nevertheless, building on our findings that increasing mesophyll conductance is possible with overexpression of SiPIP2;7, this trait will be a strong candidate to combine with complementary traits such as the overexpressing of Cytochrome *b₆f* (Ermakova et al., 2019) and Rubisco (Salesse-Smith et al., 2018), which offer improvements to photosynthesis in C₄ plants.

Materials and methods

Heterologous expression in yeast

cDNAs encoding the 12 *S. italica* aquaporins (Supplementary File 1) and *human CARBONIC ANHYDRASE II* (*hCAII*, AK312978) were codon-optimized for expression in yeast with IDT DNA tool (<https://sg.idtdna.com/pages/tools>) and a yeast related kozak sequence was added at the 5' end to help increase translation (Nakagawa, Niimura, Gojobori, Tanaka, & Miura, 2008). For CO₂ permeability measurements, pSF-TPI1-URA3 with an aquaporin and pSF-TEF1-LEU2 with *hCAII* were co-transformed into the *S. cerevisiae* strain INVSc1 (Thermo Fisher Scientific, Waltham, MA). For water permeability measurements, pSF-TPI1-URA3 with an aquaporin was transformed into the *aqy1/2* double mutant yeast strain deficient in aquaporins (Suga & Maeshima, 2004). The yeast vectors pSF-TPI1-URA3 and pSF-TEF1-LEU2 were obtained from Oxford Genetics (Oxford, UK). Yeast transformation was performed using the Frozen-EZ yeast transformation II kit (Zymo Research, Irvine, CA) and selection of positive transformants was based on amino acid complementation. To ensure CA was not limiting, CA activity was determined using a membrane inlet mass spectrometry as described by Endeward et al. (2006) (Figure 1-figure supplement 2). For CO₂ permeability measurements an average cell diameter of 4.63 μm was determined by measuring ~100 yeast cells expressing each aquaporin (Figure 1-figure supplement 2). To study the subcellular localizations of aquaporins in

yeast, a C-terminus GFP tag was added to the sequences into the pSF-TPI1-URA3 vector (pSF-TPI1-URA3-GFP). The fluorescence signal was observed using a Zeiss 780 confocal laser scanning microscope (Zeiss, Oberkochen, Germany): excitation 488 nm, emission 530 nm. Cytosolic GFP expression was used as control.

CO₂ induced intracellular acidification assay

CO₂ intracellular acidification was measured in yeast cells loaded with fluorescein diacetate (Sigma-Aldrich, St. Louis, MO) as described previously (Bertl & Kaldenhoff, 2007; Otto et al., 2010). Briefly, an overnight culture of yeast cells was collected and resuspended in an equal volume of 50 mM 4-(2-hydroxyethyl)-1-piperazineethanesulfonic acid (HEPES)-NaOH, pH 7.0, 50 μM fluorescein diacetate and incubated for 30 min in the dark at 37 °C. The suspension was centrifuged and the pellet resuspended in ice-cold incubation buffer (25 mM HEPES-NaOH, pH 6.0, 75 mM NaCl). Cells loaded with fluorescein diacetate were then injected into the stopped flow spectrophotometer (DX.17MV; Applied Photophysics, Leatherhead, UK) alongside a buffer solution (25 mM HEPES, pH 6.0, 75 mM NaHCO₃, bubbled with CO₂ for 2 h). The kinetics of acidification was measured at 490 nm excitation and >515 nm emission (OG515 long pass filter, Schott, supplied by Applied Photophysics). Data was collected over a time interval of 0.2 s and analysed using ProData SX viewer software (Applied Photophysics). CO₂ permeability was determined using the method of Yang et al. (2000). An average of 75 injections over at least three separate cultures was used for each aquaporin.

Determination of water permeability

A freeze-thaw yeast assay was used to determine water permeability of aquaporins expressed in *aqy1/2* based on previous reports (Tanghe et al., 2002). Briefly, an overnight culture was diluted to ~6x10⁶ cells (final volume 1 mL) in appropriate selection liquid growth medium and incubated at 30°C for 1 h. 250 μL of each culture were then aliquoted into two standard 1.5 mL microtubes: the first (control) tube was placed on ice and the second tube was subject to a single freeze-thaw treatment, consisting of 30-s freezing in liquid nitrogen and thawing for 20 min in a 30 °C water bath. Following the treatment, the cells were placed on ice. The tubes were then vortexed briefly to ensure even suspension of cells and 200 μL of the culture was transferred to wells of a Nunc-96 400 μL flat bottom untreated plate (Thermo Fisher Scientific, Cat#243656). Yeast growth in control and treated cultures were monitored over a 24-30 h period in a M1000 Pro plate reader (TECAN, Männedorf, Switzerland) at 30 °C with double orbital shaking at 400 rpm and measuring absorbance at 650 nm every 10 min. Growth data was log transformed and freeze-thaw survival calculated as the growth (area under the

curve) of treated culture relative to its untreated control from time zero up until the untreated control culture reached stationary phase.

For swelling assays, the coding sequence of *SiPIP2;7* was cloned into pGEMHE oocyte expression vector using LR clonase II (Thermo Fisher Scientific) and cRNA was synthesised with mMessage mMachine® T7 Transcription Kit (Thermo Fisher Scientific). *Xenopus laevis* oocytes were injected with 46 nL of RNase-free water with either no cRNA or 23 ng cRNA with a micro-injector Nanoinject II (Drummond Scientific, Broomall, PA). Post-injection oocytes were stored at 18°C in a Low Na⁺ Ringer's solution [62 mM NaCl, 36 mM KCl, 5 mM MgCl₂, 0.6 mM CaCl₂, 5 mM HEPES, 5% (v/v) horse serum (H-1270, Sigma-Aldrich) and antibiotics: 0.05 mg mL⁻¹ tetracycline, 100 units mL⁻¹ penicillin/0.1 mg mL⁻¹ streptomycin], pH 7.6 for 24–30 h. Photometric swelling assay was performed 24–30 h post-injection (Qiu, McGaughey, Groszmann, Tyerman, & Byrt, 2020).

Construct assembly and *S. viridis* transformation

The coding sequence of *S. viridis* *PIP2;7* (Sevir.2G128300.1, Phytozome, <https://phytozome.jgi.doe.gov/>) has been codon optimized for the Golden Gate cloning (Engler et al., 2014) and translationally fused with the glycine linker and the FLAG-tag coding sequence (Hopp et al., 1988). The resulting coding sequence was assembled with the *Z. mays* *PEPC* promoter and the bacterial tNos terminator into the second expression module of the pAGM4723 binary vector. The first expression module has been occupied by the hygromycin phosphotransferase (*hpt*) gene assembled with the *Oryza sativa* actin promoter and the tNos terminator. The construct was transformed into *S. viridis* cv. MEO V34-1 using *Agrobacterium tumefaciens* strain AGL1 following the procedure described in Osborn et al. (2016). T₀ plants resistant to hygromycin were transferred to soil and analyzed for SiPIP2;7-FLAG protein abundance and *hpt* insertion number by droplet digital PCR (iDNA Genetics, Norwich, UK). Lines 27, 44 and 52 were selected for further analysis because they had the strongest FLAG signal per transgene insertion number (Figure 2-figure supplement 1). The T₁ and T₂ progenies of T₀ plants 27, 44 and 52 were analyzed. Azygous T₁ plants of line 44 and their progeny were used as control.

Plant growth conditions

Seeds were surface-sterilized and germinated on medium (pH 5.7) containing 2.15 g L⁻¹ Murashige and Skoog salts, 10 mL L⁻¹ 100x Murashige and Skoog vitamins stock, 30 g L⁻¹ sucrose, 7 g L⁻¹ Phytoblend, 20 mg L⁻¹ hygromycin (no hygromycin for azygous plants). Seedlings that developed

secondary roots were transferred to 0.6 L pots with garden soil mix layered on top with 2 cm seed raising mix (Debco, Tyabb, Australia) both containing 1 g L⁻¹ Osmocote (Scotts, Bella Vista, Australia). Plants were grown in controlled environmental chambers with 16 h light/8 h dark, 28 °C day, 22 °C night, 60% humidity and ambient CO₂ concentrations. Light intensity of 300 μmol m⁻² s⁻¹ was supplied by 1000 W red sunrise 3200 K lamps (Sunmaster Growlamps, Solon, OH). Youngest fully expanded leaves of the 3–4 weeks plants before flowering were used for all analyses.

Chlorophyll and enzyme activity

Chlorophyll content was measured on frozen leaf discs homogenised with a TissueLyser II (Qiagen, Venlo, The Netherlands) (Porra, Thompson, & Kriedemann, 1989). PEPC activity was determined after Pengelly et al. (2010) from fresh leaf extracts from the plants adapted for 1 h to 800 μmol photons m⁻² s⁻¹. CA activity was measured on a membrane inlet mass spectrometer as a rate of ¹⁸O exchange from labelled ¹³C¹⁸O₂ to H₂¹⁶O at 25 °C according to von Caemmerer et al. (2004) by calculating the hydration rate after Jenkins, Furbank, and Hatch (1989). The amount of Rubisco active sites was determined by [¹⁴C] carboxyarabinitol biphosphate binding as described earlier (Ruuska, Andrews, Badger, Price, & von Caemmerer, 2000).

RNA isolation and qPCR

Leaf and root tissue were frozen in liquid N₂. Leaf samples were homogenised using a TissueLyser II and RNA was extracted using the RNeasy Plant Mini Kit (Qiagen). Roots were ground with mortar and pestle in liquid N₂ and RNA was isolated according to Massey (2012). Briefly, 150 μL of pre-heated (60 °C) extraction buffer [0.1 M trisaminomethane (Tris)-HCl, pH 8, 5 mM ethylenediaminetetraacetic acid (EDTA), 0.1 M NaCl, 0.5% sodium dodecyl sulfate (SDS), 1% 2-mercaptoethanol] was added to ~100 mg of fine root powder and incubated at 60 °C for 5 min. 150 μL of phenol:chloroform:isoamyl alcohol (25:24:1) saturated with 10 mM Tris (pH 8.0) and 1 mM EDTA was added to the samples, vortexed vigorously for 10 min and centrifuged at 4500 g for 15 min. Aqueous phase was mixed with 120 μL of isopropanol and 15 μL of 3 M sodium acetate and incubated at -80 °C for 15 min, then centrifuged at 4500 g (30 min, 4 °C). The pellet was washed twice in 300 μL of ice-cold 70% ethanol, air dried and dissolved in 60 μL of RNase-free water. After addition of 40 μL of 8 M LiCl, samples were incubated overnight at 4 °C. Nucleic acids were pelleted by centrifugation at 16,000 g (60 min, 4 °C), washed twice with 200 μL of ice-cold 70% ethanol, air dried and dissolved in RNase-free water. DNA from the samples was removed using an Ambion TURBO DNA free kit (Thermo Fisher Scientific), and RNA quality was determined using a NanoDrop (Thermo Fisher Scientific). 100 ng of total RNA were

reverse transcribed into cDNA using a SuperScript™ III Reverse Transcriptase (Thermo Fisher Scientific). qPCR and melt curve analysis were performed on a Viia7 Real-time PCR system (Thermo Fisher Scientific) using the Power SYBR green PCR Master Mix (Thermo Fisher Scientific) according to the manufacturer's protocol. Primer pairs designed to distinguish between *S. viridis* *PIP2;6* and *PIP2;7* using Primer3 in Geneious Prime (<https://www.geneious.com>) and reference primers are listed in Supplementary File 3.

Western blotting and immunolocalization

Protein isolation from leaves and gel electrophoresis were performed as described earlier (Ermakova et al., 2019). Proteins were probed with antibodies against FLAG (ab49763, 1:5000, Abcam, Cambridge, UK), RbcS (Martin-Avila et al., 2020) (1:10,000), Rieske (AS08 330, 1:3000, Agrisera, Vännäs Sweden), PEPC (AS09 458, 1:10,000, Agrisera), CA(Ludwig, von Caemmerer, Dean Price, Badger, & Furbank, 1998) (1:10,000). Quantification of immunoblots was performed with Image Lab software (Biorad, Hercules, CA). For immunolocalization leaf tissue was fixed and probed with primary antibodies against FLAG (1:40) and secondary goat anti-mouse Alexa Fluor 488-conjugated antibodies (ab150113, 1:200, Abcam) as described in Ermakova et al. (2021). Images were captured with a Zeiss 780 microscope using ZEN 2012 software (Black edition, Zeiss, Oberkochen, Germany). Images for plants of lines 27, 44 and azygous plants were acquired using online fingerprinting (488 nm excitation) with three user-defined spectral profiles for AlexaFluor488, endogenous autofluorescence and chlorophyll. The spectral profile for endogenous autofluorescence was derived from the azygous control. The image for line 52 was initially collected as a full spectral scan (490-660 nm), then linearly un-mixed using the same online fingerprint settings as previously described. Images were post-processed with FIJI (Schindelin et al., 2012), and histograms for all images were min-max adjusted.

Gas exchange measurements

Gas-exchange and fluorescence analysis were performed at an irradiance of $1500 \mu\text{mol m}^{-2} \text{s}^{-1}$ (90% red/10% blue actinic light) and different intercellular CO_2 partial pressures using a LI-6800 (LI-COR Biosciences, Lincoln, NE) equipped with a fluorometer head 6800-01 A (LI-COR Biosciences). Leaves were first equilibrated at 400 ppm CO_2 in the reference side, leaf temperature 25 °C, 60% humidity and flow rate $500 \mu\text{mol s}^{-1}$ and then a stepwise increase of CO_2 concentrations from 0 to 1600 ppm was imposed at 3 min intervals. Initial slopes of the CO_2 response curves were determined by linear fitting in OriginPro 2018b (OriginLab, Northampton, MA). Quantum yield of PSII upon the application

386 of multiphase saturating pulses ($8000 \mu\text{mol m}^{-2} \text{s}^{-1}$) was calculated according to Genty, Briantais, and
387 Baker (1989).

388 **$\text{C}^{18}\text{O}^{16}\text{O}$ discrimination measurements**

389 Simultaneous measurements of exchange of CO_2 , H_2O , $\text{C}^{18}\text{O}^{16}\text{O}$ and H_2^{18}O were made by coupling
390 two LI-6400XT gas-exchange systems to a tunable diode laser (TDL: model TGA200A, Campbell
391 Scientific Inc., Logan, UT) to measure $\text{C}^{18}\text{O}^{16}\text{O}$ discrimination and a Cavity Ring-Down Spectrometer
392 (L2130-i, Picarro Inc., Sunnyvale, CA) to measure the oxygen isotope composition of water vapor
393 (Osborn et al., 2016). Measurements were made at 2% O_2 , $380 \mu\text{mol mol}^{-1} \text{CO}_2$, leaf temperature of
394 25°C , irradiance of $1500 \mu\text{mol m}^{-2} \text{s}^{-1}$ and relative humidity of 55%. Each leaf was measured at 4 min
395 intervals and 10 readings were taken. Mesophyll conductance was calculated as described by Osborn
396 et al. (2016) with the assumptions that there was sufficient carbonic anhydrase (CA) in the mesophyll
397 cytosol for isotopic equilibration between CO_2 and HCO_3^- . We also used the calculations proposed by
398 Ogée et al. (2018) to estimate g_m . These calculations try to account for the rates of bicarbonate
399 consumption by CA. We used the rate constant of CA hydration (k_{CA}) of $6.5 \text{ mol m}^{-2} \text{s}^{-1} \text{bar}^{-1}$ for these
400 calculations.

401 **Statistical analysis**

402 One-way and two-way ANOVAs with Tukey post-hoc test were performed in OriginPro 2018b. A two-
403 tailed, heteroscedastic Student's t -tests were performed in Microsoft Excel. Linear modelling was
404 performed in R (R Core Team, 2021); mixed effects models to test the need to incorporate transgenic
405 event and copy status was performed in lme4 (Bates, Mächler, Bolker, & Walker, 2015).

406 **Acknowledgements and funding sources**

407 We thank Xueqin Wang for *S. viridis* transformation, Zac Taylor for gas-exchange measurements,
408 Murray Badger and Dimitri Tolleter for measuring CA activity in yeast, Daryl Webb, Ayla Manwaring
409 and the Centre for Advanced Microscopy at the Australian National University for confocal imaging,
410 Wendy Sullivan for help with the stopped flow spectrophotometry and Nerea Ubierna for sharing the
411 spreadsheet for the Ogée *et al.* g_m calculations. Funding information: this research was supported by
412 the Australian Research Council (ARC) Centre of Excellence for Translational Photosynthesis
413 (CE140100015). RES was funded by ARC DECRA (DE130101760). This work is presented in the
414 Australian provisional patent application # 2021900409.

415

416 **Figures and tables**

417 **Table 1.** Properties of *S. viridis* plants expressing *SiPIP2;7-FLAG* in mesophyll cells. PEPC, PEP
 418 carboxylase; Rubisco, ribulose biphosphate carboxylase oxygenase; LMA, leaf mass per area.
 419 Azygous plants of line 44 were used as control. Mean \pm SE, $n = 3$ except for biomass ($n = 8$). Three-
 420 weeks old plants before flowering were used for all analyses. No significant difference was found
 421 between the transgenic and control plants (one-way ANOVA, $\alpha = 0.05$).

422 **Figure 1.** Identification of the CO₂-permeable aquaporin *SiPIP2;7* from *S. italica*. **a.** Expression atlas of
 423 the *SiPIP* genes generated from Phytomine reported as Fragments Per Kilobase of transcript per
 424 Million mapped reads (FPKM). House-keeping genes (HK) *PROTEIN PHOSPHATASE 2A (PP2A)* and
 425 *DUAL SPECIFICITY PROTEIN (DUSP)* were included for reference. **b.** Localization of *SiPIP*-GFP fusions
 426 expressed in yeast visualised with confocal microscopy; left panels – GFP fluorescence; right panels –
 427 bright field overlaid with GFP fluorescence. Measured cell diameters are shown on Figure 1-figure
 428 supplement 2. **c.** CO₂ permeability assay on yeast co-expressing *SiPIPs* and *human CARBONIC*
 429 *ANHYDRASE II (hCAII)* analyzed by stopped flow spectrometry (see Figure 1-figure supplement 2 for
 430 details). “hCAII only” expression was used as negative control. Mean \pm SE, $n = 3$ biological replicates.
 431 Two independent experiments are presented. Asterisks indicate statistically significant differences
 432 between yeast expressing *SiPIPs* and “hCAII only” control (t -test, $p < 0.05$). **d.** Yeast water
 433 permeability assessed in the yeast aquaporin deletion background (*aqy1 aqy2*) by the cumulative
 434 growth between untreated and freeze-thawed cells and determined by the percent area under the
 435 curve (% AUC). The yeast expressing the β -glucuronidase reporter gene (515.GUS) was used as
 436 negative control. Mean \pm SE, $n = 4$ biological replicates. Asterisks indicate statistically significant
 437 differences between yeast expressing *SiPIPs* and 515.GUS control (t -test, $p < 0.01$).

438 **Figure 2.** Characterization of *S. viridis* plants expressing *SiPIP2;7-FLAG* in mesophyll cells. **a.**
 439 Immunodetection of *SiPIP2;7-FLAG* and photosynthetic proteins in leaf protein samples loaded on
 440 leaf area basis. Three plants from each of the three transgenic lines were analyzed and dilution series
 441 of the control and line 44-3 samples were used for relative quantification. **b.** Protein abundances
 442 calculated from the immunoblots relative to control plants. Mean \pm SE. No significant difference was
 443 found between the transgenic and control plants (t -test). **c.** Immunolocalisation of *SiPIP2;7-FLAG* on
 444 leaf cross-sections visualized with confocal microscopy. Fluorescence signals are pseudo-colored:
 445 green - FLAG antibodies labelled with secondary antibodies conjugated with Alexa Fluor 488; red -
 446 chlorophyll autofluorescence. BS, bundle sheath cell; M, mesophyll cell. Scale bars = 20 μ m. Azygous

plants of line 44 were used as control. Uncropped images of the blots are provided in Figure 2 - source data 1-5.

Figure 3. CO₂ response of CO₂ assimilation rate (**a**) and quantum yield of Photosystem II (**b**) in *S. viridis* plants expressing *SiPIP2;7-FLAG* in mesophyll cells. Measurements were performed at the irradiance of 1500 μmol m⁻² s⁻¹; azygous plants of line 44 were used as control. Mean ± SE, *n* = 4-6 biological replicates. No significant difference was found between the transgenic and control plants (one-way ANOVA, α = 0.05).

Figure 4. Effect of the mesophyll conductance, *g_m*, on the initial slope of the CO₂ assimilation response curve to the intercellular CO₂ partial pressure (*AC_i* curve) in leaves of *S. viridis* expressing *SiPIP2;7-FLAG* in mesophyll cells. **a.** Initial slope of the *AC_i* curves estimated by linear fitting of curves (a subset of curves is presented in Figure 3a inset). **b.** Mesophyll conductance, *g_m*, estimated by oxygen isotope discrimination assuming full isotopic equilibrium (Osborn et al., 2016). Measurements were made at ambient CO₂ and low O₂. **c.** Data from a and b compared to the C₄ biochemical model predictions (von Caemmerer, 2000; von Caemmerer & Furbank, 1999). All graphs show Mean ± SE; azygous plants of line 44 were used as control. The model relates the initial slope of the *AC_i* curve (*dA/C_i*) to *g_m* by: $\frac{dA}{dC_i} = g_m V_{pmax} / (g_m K_p + V_{pmax})$, where *V_{pmax}* and *K_p* denote the maximum PEPC activity and the Michaelis Menten constant for CO₂ taken here as 250 μmol m⁻² s⁻¹ and 82 μbar (DiMario & Cousins, 2019; von Caemmerer, 2021). Asterisks indicate statistically significant differences between the plants of lines 27 (*p* = 0.04573) and 44 (*p* = 0.03724) and control plants (Two-way ANOVA with Tukey post-hoc test, α = 0.05). Plants of line 52 were not significantly different from the control plants (*p* = 0.27518).

Supplementary Figures

Figure 1-figure supplement 1. Phylogenetic analysis of *S. italica* PIP protein sequences. Amino acid sequences for the PIP1 and PIP2 proteins from *Setaria italica* were acquired from Phytozome and numbered based on McGaughey et al. (2016). The protein sequences were aligned using MUSCLE in Geneious (v 11.1.5) and the phylogenetic tree generated using the neighbour-joining method with pairwise deletions in MEGA10 (Kumar, Stecher, Li, Knyaz, & Tamura, 2018).

Figure 1-figure supplement 2. Expression of *S. italica* PIPs in yeast for functional testing of CO₂ permeability. **a.** Schematic highlighting the yeast expression system and the detection of CO₂ permeability by measuring the change in fluorescein fluorescence due to the acidification of the

cytoplasm by producing protons from the hydration of CO₂ from ectopically expressed carbonic anhydrase. The decline in fluorescence is measured by stop-flow spectrophotometry at 490nm. **b.** Construct design used for expression and assay of CO₂ permeability and localisation in yeast. **c.** CA activity measured in yeast cells expressing PIPs. **d.** The cell diameter of yeast cells expressing PIPs.

Figure 1-figure supplement 3. CO₂ transport capacity of SiPIP2;7 is not confounded by permeability of protons. The changes in CO₂ permeability, detected on the stopped flow spectrophotometer (Figure 1c), could be confounded by other factors such as permeability to protons also causing intracellular acidification. When SiPIP2;7 + hCAII (black) and hCAII alone (red) were injected alongside CO₂ enriched buffer, a decrease in pH was observed. This decrease was more pronounced in PIP2;7 + hCAII indicating higher CO₂ transport rate. When SiPIP2;7 + hCAII and hCAII were injected with a low pH (*i.e.* proton rich) buffer, no decrease in fluorescence intensity was observed with either SiPIP2;7 + hCAII (grey) or hCAII alone (pink) demonstrating that the decrease in fluorescence seen with the CO₂ enriched was not due to proton movement through the membrane. In fact, both traces were the same specifically pointing out that SiPIP2;7 expression did not cause excessive proton movement which could lead to a false-positive result for CO₂ permeability.

Figure 1-figure supplement 4. SiPIP2;7 is a functional water channel when expressed in *X. laevis* oocytes. Oocytes were injected with either water (control) or 23 ng of *SiPIP2;7* cRNA. Osmotic permeability (P_{os}) was determined via photometric swelling where oocytes were pre-incubated in the isotonic swelling solution before being transferred to the hypotonic swelling solution for the assay. Mean \pm SE, $P < 0.0001$ (*t*-test).

Figure 2-figure supplement 1. Immunodetection of SiPIP2;7-FLAG in leaves of transgenic *S. viridis* plants. **a.** T₀ plants; T-DNA insertion numbers indicate the number of *hpt* gene copies detected by droplet digital PCR. Lines selected for further analysis are marked with asterisks. **b.** Homozygous T₃ plants; azygous plants of line 44 were used as control. Uncropped images of the blots from (a) are provided in Figure S5 – source data 1-4; uncropped images of the blot from (b) are provided in Figure 2 – source data 1-2.

Figure 2-figure supplement 2. qPCR analysis of *SiPIP2;6* and *SiPIP2;7* expression in leaves and roots of control and transgenic *S. viridis* plants. Azygous plants of line 44 were used as control.

Figure 3-figure supplement 1. Stomatal conductance to water vapor (g_{sw}) measured at different intercellular CO_2 partial pressure. No significant differences were detected between the transgenic and control plants (One-way ANOVA, $\alpha = 0.05$).

Figure 3-figure supplement 2. The relationship between the relative abundance of SiPIP2;7 and the initial slopes or the maximum assimilation rates (A_{max}) of the AC_i curves in individual T_1 plants of four transgenic lines. **a.** Immunodetection of the SiPIP2;7-FLAG in plants is on a leaf area basis. Quantification of immunoblot band intensities is shown underneath the bands in relative units. **b.** The initial slopes compared to the relative SiPIP2;7 content. A second order polynomial was fitted using R, producing an R^2 of 0.345 ($p < 0.05$, $F = 5.007$, $df = 2$ and 19), which was significantly better than a linear fit when compared using ANOVA ($p < 0.05$). No significant improvement of the model could be found adding random effects to account for transformation event or zygosity of lines. Both polynomial coefficients were significant to the model ($p < 0.05$). **c.** A_{max} compared to the relative SiPIP2;7 content. A linear model was fitted using R. No significant effects could be found, with R^2 of the model being only 0.065; addition of random terms to this analysis were not found to be of any advantage.

Figure 4-figure supplement 1. Comparison of the g_m estimated by oxygen isotope discrimination assuming full isotopic equilibrium (Osborn et al., 2016) and calculations suggested by (Ogée et al., 2018).

Supplementary Files

Supplementary File 1. Amino acid similarity of *S. italica* and *S. viridis* PIPs.

Supplementary File 2. Amino acid composition of *S. italica* PIPs at known substrate selectivity positions. Aquaporins have six transmembrane α -helices (H1-H6) joined by five loops (LA-LE). The monomeric channel is characterized by two NPA (Asn, Pro, Ala) motifs on loops A and E and along with the aromatic/arginine selectivity filter, these largely dictate the transport selectivity of substrates through the monomeric channels (Azad et al., 2016). Froger's positions indicate additional residues that are predicted for substrate specificity (Froger, Tallur, Thomas, & Delamarche, 1998).

Supplementary File 3. Primers used for qPCR.

Source data

Figure 1 - Source data 1. Gene expression and yeast assays

534 **Figure 2 - Source data 1-5.** Uncropped images of western blots
535 **Figure 3 - Source data 1.** Gas-exchange and fluorescence analysis
536 **Figure 2-figure supplement 1 - Source data 1-4.** Uncropped images of western blots
537 **Figure 3-figure supplement 2 - Source data 1-3.** Uncropped images of western blots
538

539 References

- 540 Azad, A. K., Ahmed, J., Alum, M. A., Hasan, M. M., Ishikawa, T., Sawa, Y., & Katsuhara, M. (2016). Genome-
541 Wide Characterization of Major Intrinsic Proteins in Four Grass Plants and Their Non-Aqua Transport
542 Selectivity Profiles with Comparative Perspective. *PLOS ONE*, 11(6), e0157735.
543 doi:10.1371/journal.pone.0157735
- 544 Barbour, M. M., Evans, J. R., Simonin, K. A., & von Caemmerer, S. (2016). Online CO₂ and H₂O oxygen isotope
545 fractionation allows estimation of mesophyll conductance in C₄ plants, and reveals that mesophyll
546 conductance decreases as leaves age in both C₄ and C₃ plants. *New Phytologist*, 210, 875-889
547 doi:10.1111/nph.13830
- 548 Bates, D., Mächler, M., Bolker, B., & Walker, S. (2015). Fitting Linear Mixed-Effects Models Using lme4. *Journal*
549 *of Statistical Software*, 67(1), 1 - 48. doi:10.18637/jss.v067.i01
- 550 Berny, Marie C., Gilis, D., Rومان, M., & Chaumont, F. (2016). Single Mutations in the Transmembrane
551 Domains of Maize Plasma Membrane Aquaporins Affect the Activity of Monomers within a
552 Heterotetramer. *Molecular Plant*, 9(7), 986-1003. doi:<https://doi.org/10.1016/j.molp.2016.04.006>
- 553 Bertl, A., & Kaldenhoff, R. (2007). Function of a separate NH₃-pore in Aquaporin TIP2;2 from wheat. *FEBS*
554 *Letters*, 581(28), 5413-5417. doi:<https://doi.org/10.1016/j.febslet.2007.10.034>
- 555 Brutnell, T. P., Wang, L., Swartwood, K., Goldschmidt, A., Jackson, D., Zhu, X.-G., . . . Van Eck, J. (2010). *Setaria*
556 *viridis*: a model for C₄ photosynthesis. *The Plant Cell Online*, 22(8), 2537-2544.
- 557 Chaumont, F., Barrieu, F., Jung, R., & Chrispeels, M. J. (2000). Plasma Membrane Intrinsic Proteins from Maize
558 Cluster in Two Sequence Subgroups with Differential Aquaporin Activity. *Plant physiology*, 122(4),
559 1025. doi:10.1104/pp.122.4.1025
- 560 Chaumont, F., Barrieu, F., Wojcik, E., Chrispeels, M. J., & Jung, R. (2001). Aquaporins Constitute a Large and
561 Highly Divergent Protein Family in Maize. *Plant Physiology*, 125(3), 1206. doi:10.1104/pp.125.3.1206
- 562 Cousins, A. B., Mullendore, D. L., & Sonawane, B. V. (2020). Recent developments in mesophyll conductance in
563 C₃, C₄, and crassulacean acid metabolism plants. *The Plant Journal*, 101(4), 816-830.
564 doi:<https://doi.org/10.1111/tpj.14664>
- 565 De Rosa, A., Watson-Lazowski, A., Evans, J. R., & Groszmann, M. (2020). Genome-wide identification and
566 characterisation of Aquaporins in *Nicotiana tabacum* and their relationships with other Solanaceae
567 species. *BMC Plant Biology*, 20(1), 266. doi:10.1186/s12870-020-02412-5
- 568 DiMario, R. J., & Cousins, A. B. (2019). A single serine to alanine substitution decreases bicarbonate affinity of
569 phosphoenolpyruvate carboxylase in *C4Flaveria trinervia*. *Journal of Experimental Botany*, 70(3), 995-
570 1004. doi:10.1093/jxb/ery403
- 571 Ding, X., Matsumoto, T., Gena, P., Liu, C., Pellegrini-Calace, M., Zhong, S., . . . Calamita, G. (2013). Water and
572 CO₂ permeability of SsAqpZ, the cyanobacterium *Synechococcus* sp. PCC7942 aquaporin. *Biology of*
573 *the Cell*, 105(3), 118-128. doi:<https://doi.org/10.1111/boc.201200057>
- 574 Endeward, V., Musa-Aziz, R., Cooper, G. J., Chen, L. M., Pelletier, M. F., Virkki, L. V., . . . Gros, G. (2006).
575 Evidence that aquaporin 1 is a major pathway for CO₂ transport across the human erythrocyte
576 membrane. *The FASEB Journal*, 20(12), 1974-1981. doi:<https://doi.org/10.1096/fj.04-3300com>
- 577 Engler, C., Youles, M., Gruetzner, R., Ehnert, T.-M., Werner, S., Jones, J. D. G., . . . Marillonnet, S. (2014). A
578 Golden Gate Modular Cloning Toolbox for Plants. *ACS Synthetic Biology*, 3(11), 839-843.
579 doi:10.1021/sb4001504
- 580 Ermakova, M., Arrivault, S., Giuliani, R., Danila, F., Alonso-Cantabrana, H., Vlad, D., . . . Furbank, R. T. (2021).
581 Installation of C₄ photosynthetic pathway enzymes in rice using a single construct. *Plant Biotechnology*
582 *Journal*, doi:<https://doi.org/10.1111/pbi.13487>. doi:<https://doi.org/10.1111/pbi.13487>
- 583 Ermakova, M., Lopez-Calcano, P. E., Raines, C. A., Furbank, R. T., & von Caemmerer, S. (2019). Overexpression
584 of the Rieske FeS protein of the Cytochrome b₆f complex increases C₄ photosynthesis in *Setaria viridis*.
585 *Communications Biology* 2(314). doi:<https://doi.org/10.1038/s42003-019-0561-9>
- 586 Evans, J. R., & von Caemmerer, S. (1996). Carbon dioxide diffusion inside leaves. *Plant physiology*, 110(2), 339-
587 346. Retrieved from <Go to ISI>://A1996TW20800001

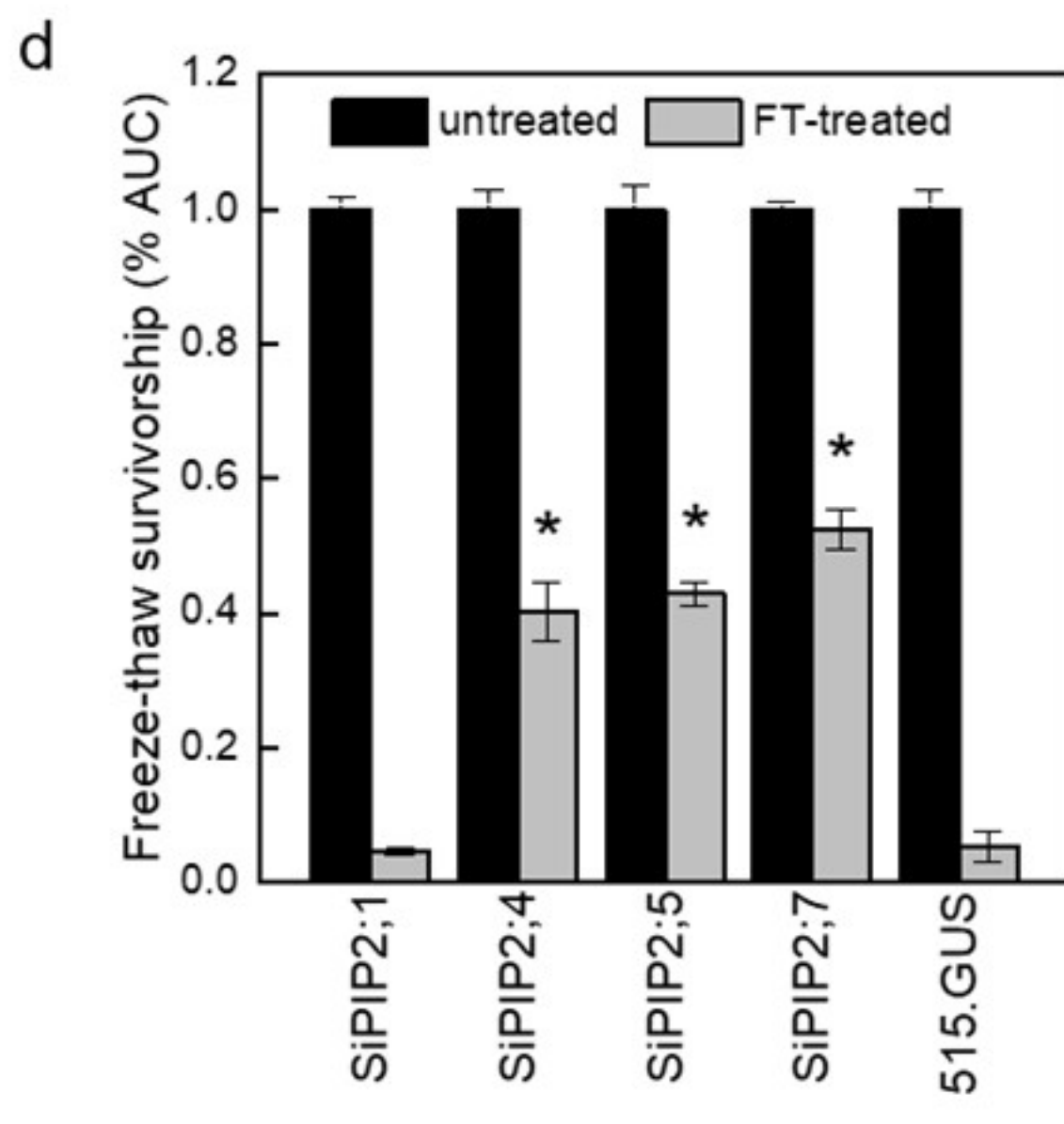
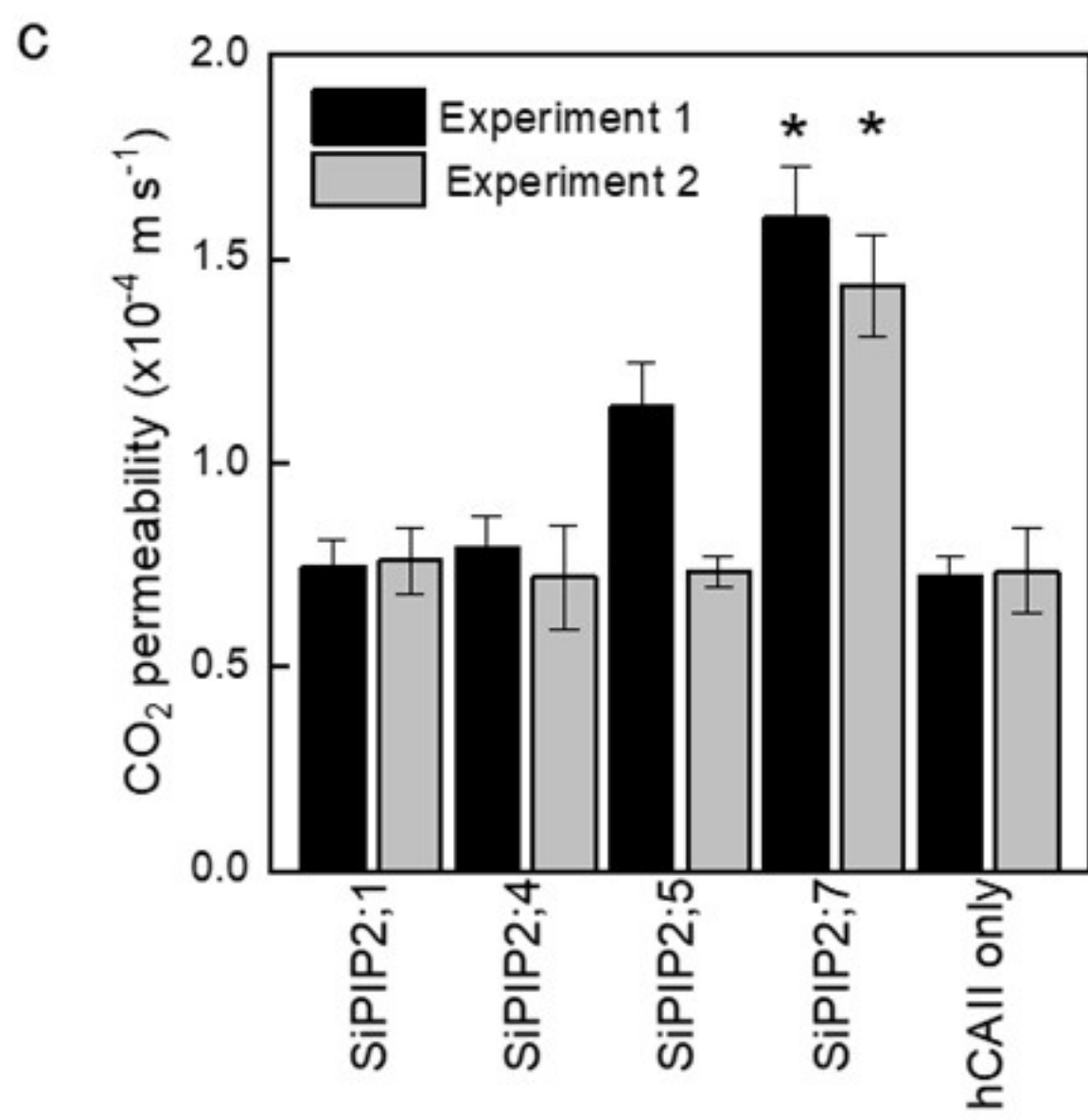
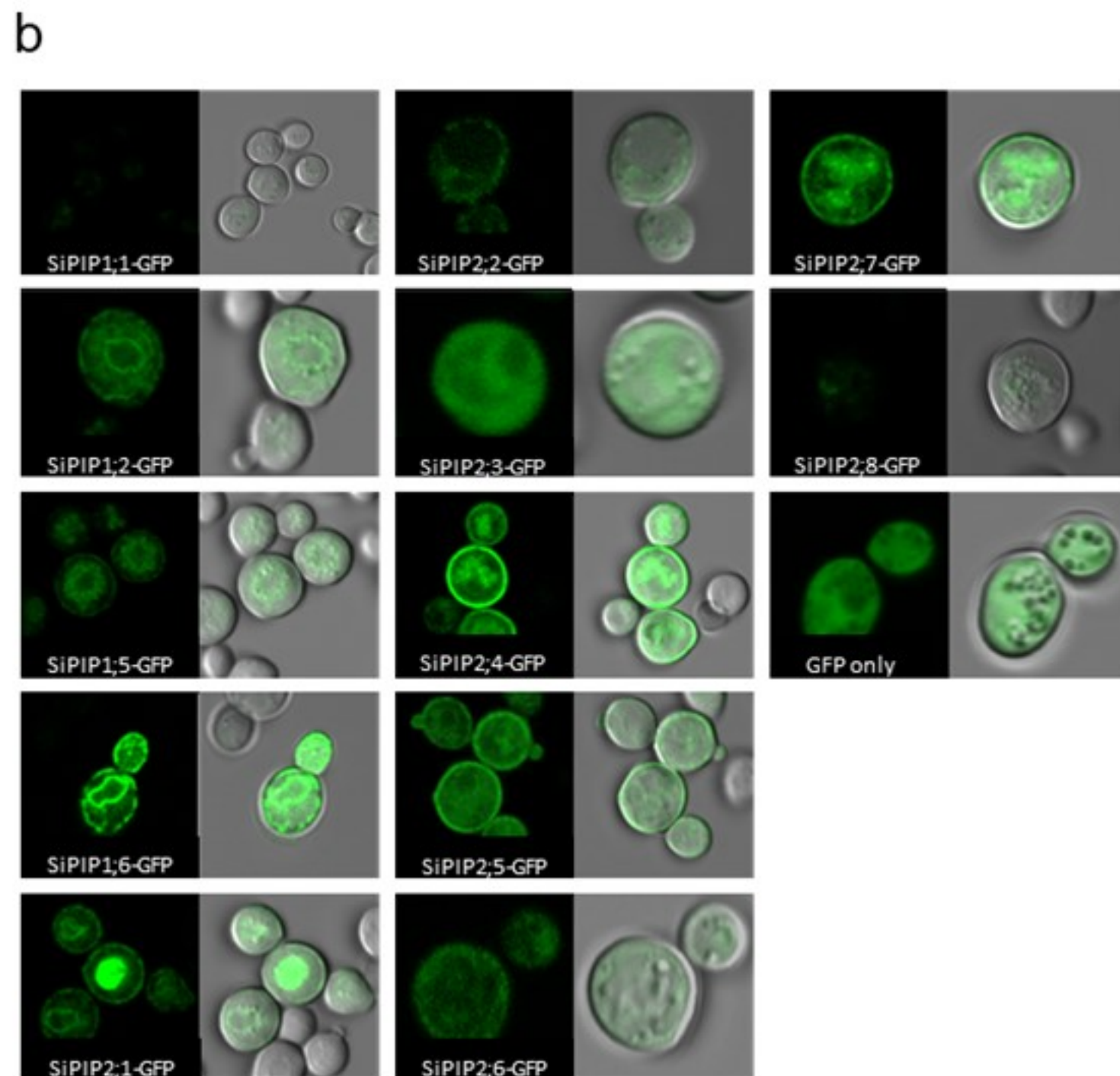
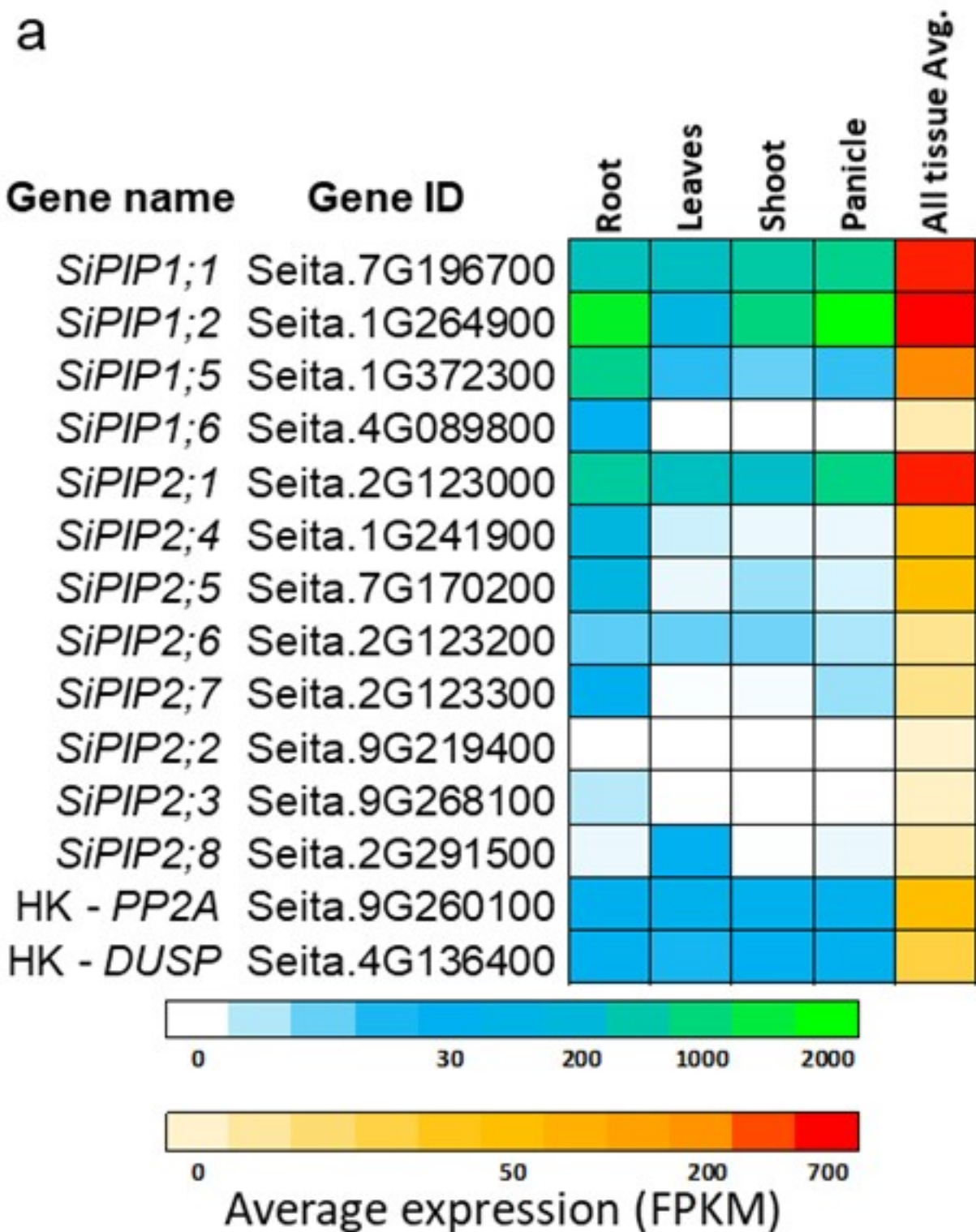
- Fernández-San Millán, A., Aranjuelo, I., Douthe, C., Nadal, M., Ancín, M., Larraya, L., . . . Veramendi, J. (2018). Physiological performance of transplastomic tobacco plants overexpressing aquaporin AQP1 in chloroplast membranes. *Journal of Experimental Botany*, 69(15), 3661-3673. doi:10.1093/jxb/ery148
- Flexas, J., Ribas-Carbó, M., Hanson, D. T., Bota, J., Otto, B., Cifre, J., . . . Kaldenhoff, R. (2006). Tobacco aquaporin NtAQP1 is involved in mesophyll conductance to CO₂ in vivo. *The Plant Journal*, 48(3), 427-439. doi:10.1111/j.1365-3113.2006.02879.x
- Froger, A., Tallur, B., Thomas, D., & Delamarche, C. (1998). Prediction of functional residues in water channels and related proteins. *Protein science : a publication of the Protein Society*, 7(6), 1458-1468. doi:10.1002/pro.5560070623
- Gambetta, G. A., Knipfer, T., Fricke, W., & McElrone, A. J. (2017). Aquaporins and root water uptake. In *Plant aquaporins* (pp. 133-153). Cham: Springer.
- Genty, B., Briantais, J.-M., & Baker, N. (1989). The relationship between the quantum yield of photosynthetic electron transport and quenching of chlorophyll fluorescence. *Biochimica et Biophysica Acta*, 990, 87-92.
- Groszmann, M., Osborn, H. L., & Evans, J. R. (2017). Carbon dioxide and water transport through plant aquaporins. *Plant, Cell & Environment*, 40(6), 938-961. doi:<https://doi.org/10.1111/pce.12844>
- Gupta, S. D., Levey, M., Schulze, S., Karki, S., Emmerling, J., Streubel, M., . . . Westhoff, P. (2020). The C4Ppc promoters of many C4 grass species share a common regulatory mechanism for gene expression in the mesophyll cell. *The Plant Journal*, 101(1), 204-216. doi:10.1111/tpj.14532
- Hanba, Y. T., Shibasaka, M., Hayashi, Y., Hayakawa, T., Kasamo, K., Terashima, I., & Katsuhara, M. (2004). Overexpression of the Barley Aquaporin HvPIP2;1 Increases Internal CO₂ Conductance and CO₂ Assimilation in the Leaves of Transgenic Rice Plants. *Plant and Cell Physiology*, 45(5), 521-529. doi:10.1093/pcp/pch070
- Heckwolf, M., Pater, D., Hanson, D. T., & Kaldenhoff, R. (2011). The Arabidopsis thaliana aquaporin AtPIP1;2 is a physiologically relevant CO₂ transport facilitator. *Plant Journal*, 67(5), 795-804. Retrieved from <Go to ISI>://WOS:000294827700005
- Heinen, R. B., Bienert, G. P., Cohen, D., Chevalier, A. S., Uehlein, N., Hachez, C., . . . Chaumont, F. (2014). Expression and characterization of plasma membrane aquaporins in stomatal complexes of Zea mays. *Plant Molecular Biology*, 86(3), 335-350. doi:10.1007/s11103-014-0232-7
- Hibberd, J. M., & Quick, W. P. (2002). Characteristics of C4 photosynthesis in stems and petioles of C3 flowering plants. *Nature*, 415(6870), 451-454.
- Hopp, T. P., Prickett, K. S., Price, V. L., Libby, R. T., March, C. J., Pat Cerretti, D., . . . Conlon, P. J. (1988). A Short Polypeptide Marker Sequence Useful for Recombinant Protein Identification and Purification. *Bio/Technology*, 6(10), 1204-1210. doi:10.1038/nbt1088-1204
- Jenkins, C. L., Furbank, R. T., & Hatch, M. D. (1989). Mechanism of C4 photosynthesis: a model describing the inorganic carbon pool in bundle sheath cells. *Plant physiology*, 91(4), 1372-1381.
- Kaldenhoff, R. (2012). Mechanisms underlying CO₂ diffusion in leaves. *Current Opinion in Plant Biology*, 15(3), 276-281. doi:<http://dx.doi.org/10.1016/j.pbi.2012.01.011>
- Kromdijk, J., Głowacka, K., & Long, S. P. (2020). Photosynthetic efficiency and mesophyll conductance are unaffected in Arabidopsis thaliana aquaporin knock-out lines. *Journal of Experimental Botany*, 71(1), 318-329. doi:10.1093/jxb/erz442
- Kumar, S., Stecher, G., Li, M., Knyaz, C., & Tamura, K. (2018). MEGA X: Molecular Evolutionary Genetics Analysis across Computing Platforms. *Molecular Biology and Evolution*, 35(6), 1547-1549. doi:10.1093/molbev/msy096
- Ludwig, M., von Caemmerer, S., Dean Price, G., Badger, M. R., & Furbank, R. T. (1998). Expression of Tobacco Carbonic Anhydrase in the C₄ Dicot *Flaveria bidentis* Leads to Increased Leakiness of the Bundle Sheath and a Defective CO₂-Concentrating Mechanism. *Plant Physiology*, 117(3), 1071. doi:10.1104/pp.117.3.1071
- Martin-Avila, E., Lim, Y.-L., Birch, R., Dirk, L. M. A., Buck, S., Rhodes, T., . . . Whitney, S. M. (2020). Modifying Plant Photosynthesis and Growth via Simultaneous Chloroplast Transformation of Rubisco Large and Small Subunits. *The Plant Cell*, 32(9), 2898. doi:10.1105/tpc.20.00288

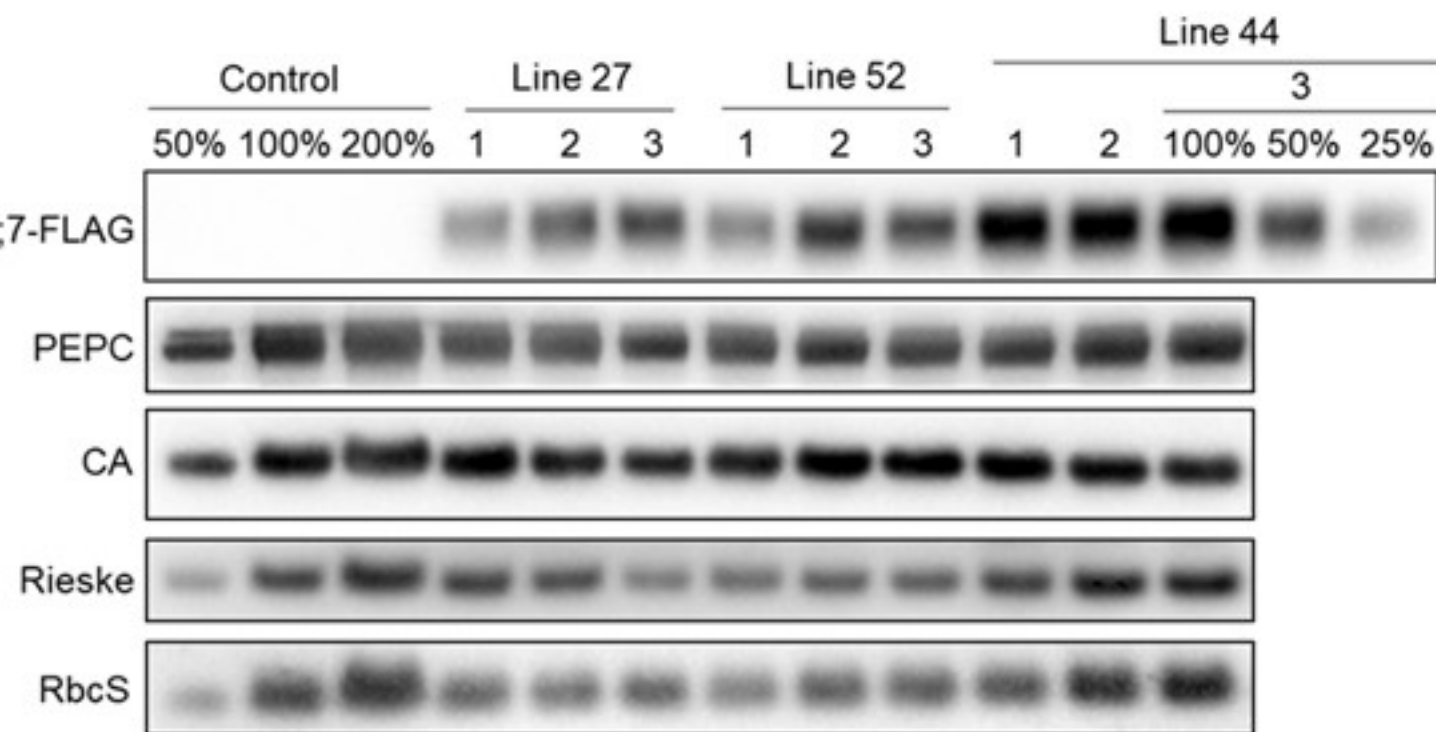
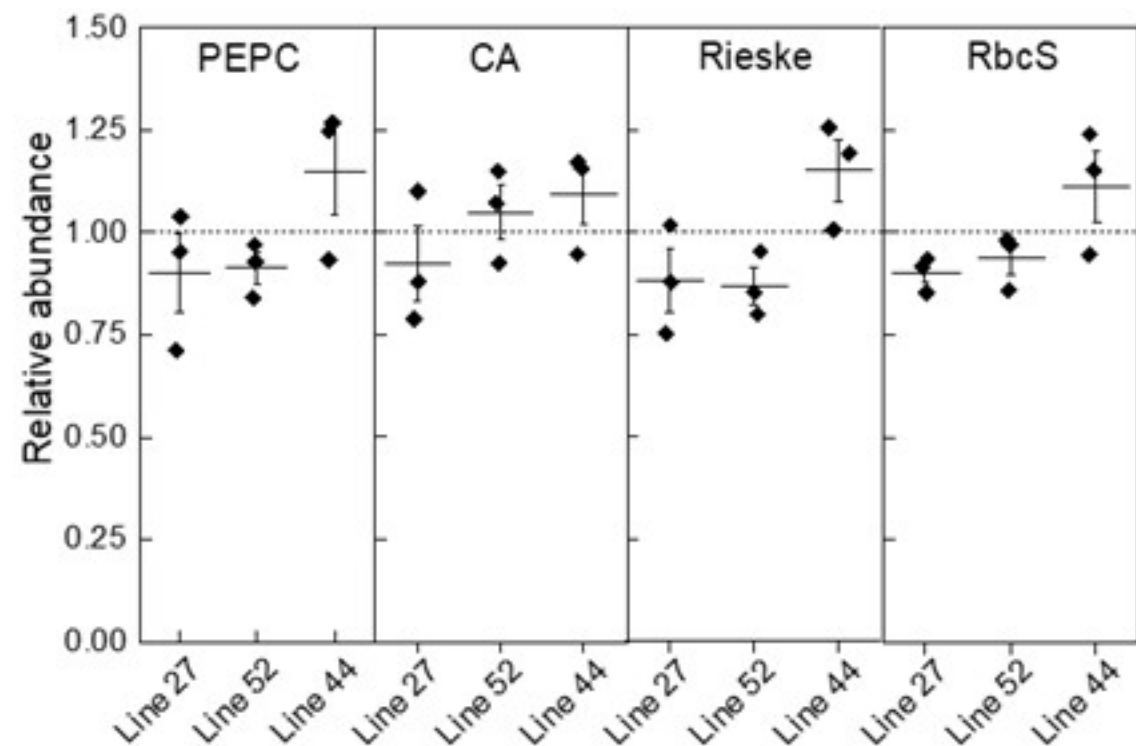
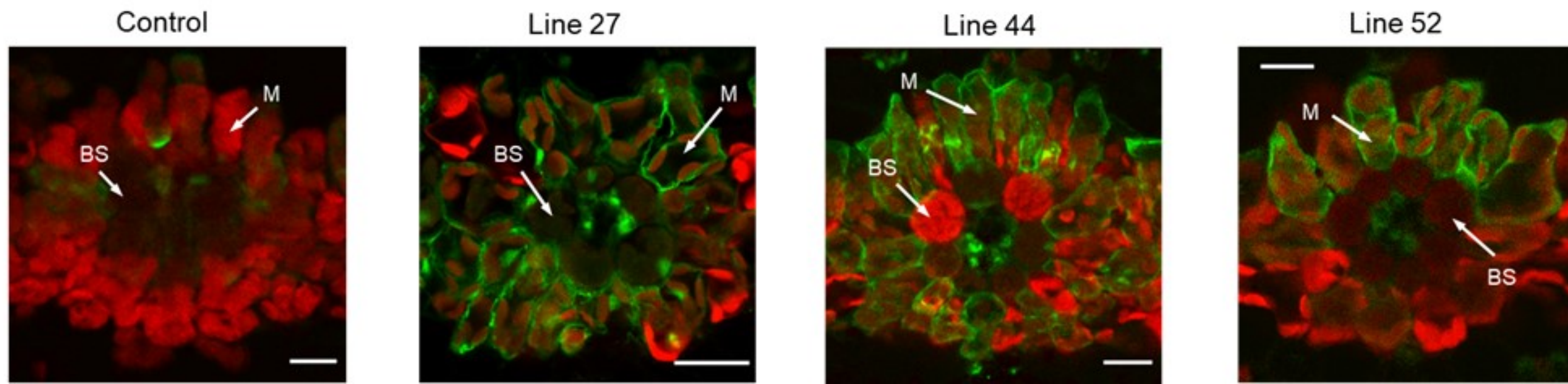
- Massey, B. (2012). *Understanding betalain regulation in floral and vegetative tissues of Ptilotus cultivars*. The University of Queensland, School of Agriculture and Food Sciences.
- McGaughey, S. A., Osborn, H. L., Chen, L., Pegler, J. L., Tyerman, S. D., Furbank, R. T., . . . Grof, C. P. L. (2016). Roles of Aquaporins in *Setaria viridis* Stem Development and Sugar Storage. *Frontiers in plant science*, 7(1815). doi:10.3389/fpls.2016.01815
- McGaughey, S. A., Qiu, J., Tyerman, S. D., & Byrt, C. S. (2018). Regulating Root Aquaporin Function in Response to Changes in Salinity. In *Annual Plant Reviews online* (pp. 381-416).
- Mori, I. C., Rhee, J., Shibasaka, M., Sasano, S., Kaneko, T., Horie, T., & Katsuhara, M. (2014). CO₂ Transport by PIP2 Aquaporins of Barley. *Plant and Cell Physiology*, 55(2), 251-257. doi:10.1093/pcp/pcu003
- Mukhopadhyay, R., Bhattacharjee, H., & Rosen, B. P. (2014). Aquaglyceroporins: generalized metalloid channels. *Biochimica et biophysica acta*, 1840(5), 1583-1591. doi:10.1016/j.bbagen.2013.11.021
- Nakagawa, S., Niimura, Y., Gojobori, T., Tanaka, H., & Miura, K.-i. (2008). Diversity of preferred nucleotide sequences around the translation initiation codon in eukaryote genomes. *Nucleic Acids Research*, 36(3), 861-871. doi:10.1093/nar/gkm1102
- Ogée, J., Wingate, L., & Genty, B. (2018). Estimating mesophyll conductance from measurements of C¹⁸OO discrimination and carbonic anhydrase activity. *Plant Physiology*, 178(2), 728-752. doi:10.1104/pp.17.01031
- Osborn, H. L., Alonso-Cantabrana, H., Sharwood, R. E., Covshoff, S., Evans, J. R., Furbank, R. T., & von Caemmerer, S. (2016). Effects of reduced carbonic anhydrase activity on CO₂ assimilation rates in *Setaria viridis*: a transgenic analysis. *Journal of Experimental Botany*, 68(2), 299-310. doi:10.1093/jxb/erw357
- Otto, B., Uehlein, N., Sdorra, S., Fischer, M., Ayaz, M., Belastegui-Macadam, X., . . . Kaldenhoff, R. (2010). Aquaporin Tetramer Composition Modifies the Function of Tobacco Aquaporins. *Journal of Biological Chemistry*, 285(41), 31253-31260.
- Pengelly, J. J. L., Sirault, X. R. R., Tazoe, Y., Evans, J. R., Furbank, R. T., & von Caemmerer, S. (2010). Growth of the C₄ dicot *Flaveria bidentis*: photosynthetic acclimation to low light through shifts in leaf anatomy and biochemistry. *Journal of Experimental Botany*, 61(14), 4109-4122.
- Perez Di Giorgio, J., Soto, G., Alleva, K., Jozefkowicz, C., Amodeo, G., Muschietti, J. P., & Ayub, N. D. (2014). Prediction of Aquaporin Function by Integrating Evolutionary and Functional Analyses. *The Journal of Membrane Biology*, 247(2), 107-125. doi:10.1007/s00232-013-9618-8
- Pfeffer, M., & Peisker, M. (1995). *In vivo* K_m for CO₂ (K_p) of phosphoenolpyruvate carboxylase (PEPC) and mesophyll CO₂ transport resistance (r_m) in leaves of *Zea mays* L. In P. Mathis (Ed.), *Photosynthesis: from light to biosphere* (Vol. V, pp. 547-550): Kluwer Academic Publishers.
- Porra, R. J., Thompson, W. A., & Kriedemann, P. E. (1989). Determination of accurate extinction coefficients and simultaneous equations for assaying chlorophylls a and b extracted with four different solvents: verification of the concentration of chlorophyll standards by atomic absorption spectroscopy. *Biochimica et Biophysica Acta (BBA) - Bioenergetics*, 975(3), 384-394. doi:[https://doi.org/10.1016/S0005-2728\(89\)80347-0](https://doi.org/10.1016/S0005-2728(89)80347-0)
- Qiu, J., McGaughey, S. A., Groszmann, M., Tyerman, S. D., & Byrt, C. S. (2020). Phosphorylation influences water and ion channel function of AtPIP2;1. *Plant, Cell & Environment*, 43(10), 2428-2442. doi:<https://doi.org/10.1111/pce.13851>
- Ruuska, S. A., Andrews, T. J., Badger, M. R., Price, G. D., & von Caemmerer, S. (2000). The role of chloroplast electron transport and metabolites in modulating Rubisco activity in tobacco. Insights from transgenic plants with reduced amounts of cytochrome b/f complex or glyceraldehyde 3-phosphate dehydrogenase. *Plant physiology*, 122(2), 491-504.
- Sade, N., Gebretsadik, M., Seligmann, R., Schwartz, A., Wallach, R., & Moshelion, M. (2010). The Role of Tobacco Aquaporin1 in Improving Water Use Efficiency, Hydraulic Conductivity, and Yield Production Under Salt Stress. *Plant physiology*, 152(1), 245. doi:10.1104/pp.109.145854
- Salesse-Smith, C. E., Sharwood, R. E., Busch, F. A., Kromdijk, J., Bardal, V., & Stern, D. B. (2018). Overexpression of Rubisco subunits with RAF1 increases Rubisco content in maize. *Nature Plants*, 4(10), 802-810. doi:10.1038/s41477-018-0252-4

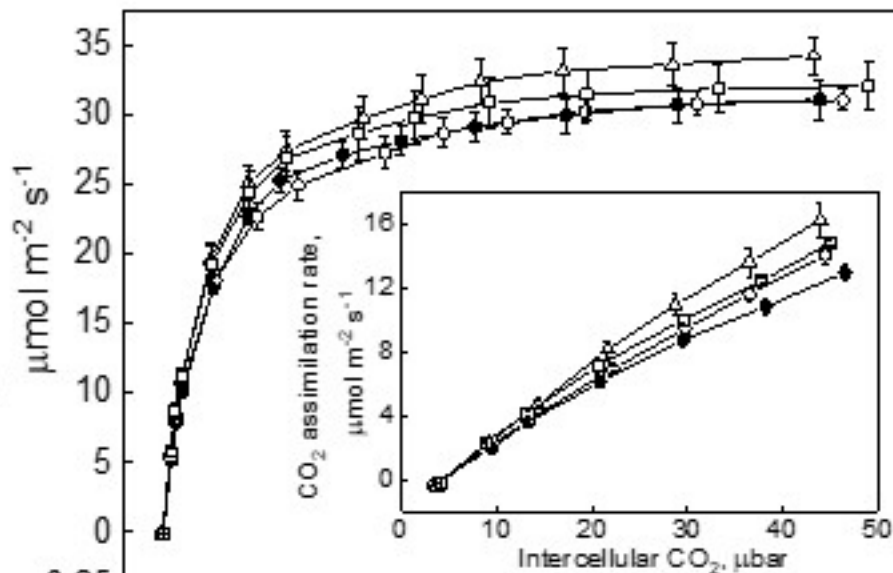
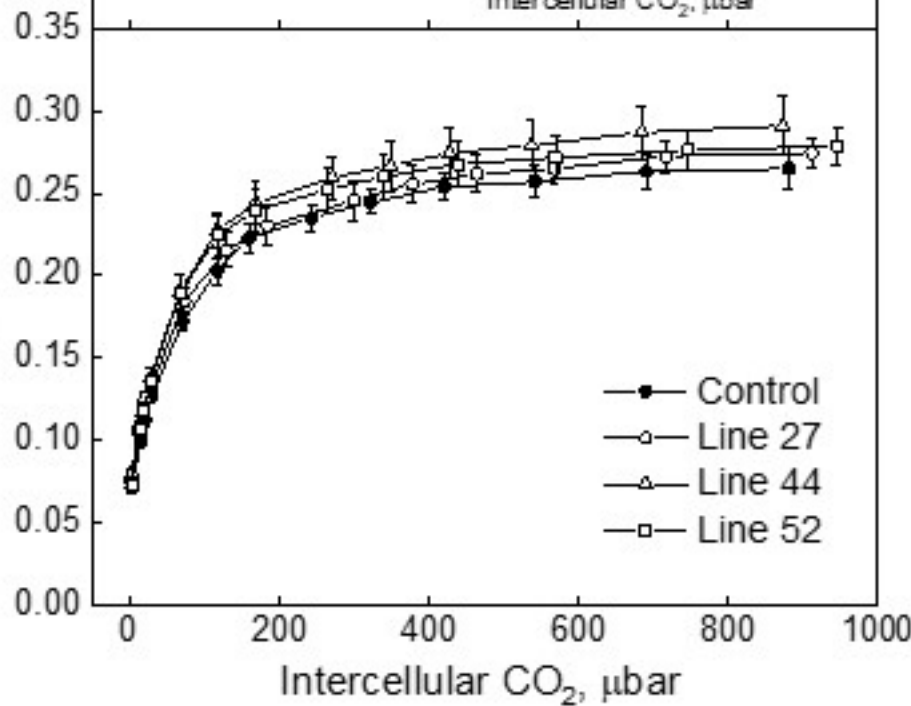
- Schindelin, J., Arganda-Carreras, I., Frise, E., Kaynig, V., Longair, M., Pietzsch, T., . . . Cardona, A. (2012). Fiji: an open-source platform for biological-image analysis. *Nature Methods*, 9(7), 676-682. doi:10.1038/nmeth.2019
- Stemmet, M. C., De Bruyn, J. A., & Zeeman, P. B. (1962). THE UPTAKE OF CARBON DIOXIDE BY PLANT ROOTS. *Plant and Soil*, 17(3), 357-364. Retrieved from <http://www.jstor.org/stable/42931981>
- Suga, S., & Maeshima, M. (2004). Water Channel Activity of Radish Plasma Membrane Aquaporins Heterologously Expressed in Yeast and Their Modification by Site-Directed Mutagenesis. *Plant and Cell Physiology*, 45(7), 823-830. doi:10.1093/pcp/pch120
- Tanghe, A., Van Dijck, P., Dumortier, F., Teunissen, A., Hohmann, S., & Thevelein, J. M. (2002). Aquaporin expression correlates with freeze tolerance in baker's yeast, and overexpression improves freeze tolerance in industrial strains. *Applied and environmental microbiology*, 68(12), 5981-5989. doi:10.1128/aem.68.12.5981-5989.2002
- Tyerman, S. D., McGaughey, S. A., Qiu, J., Yool, A. J., & Byrt, C. S. (2021). Adaptable and multifunctional ion-conducting aquaporins. *Annual Review of Plant Biology*, 72. doi:10.1146/annurev-arplant-081720-013608
- Ubierna, N., Gandin, A., Boyd, R. A., & Cousins, A. B. (2017). Temperature response of mesophyll conductance in three C₄ species calculated with two methods: ¹⁸O discrimination and in vitro V_{pmax}. *New Phytologist*, 214(1), 66-80. doi:10.1111/nph.14359
- Uehlein, N., Kai, L., & Kaldenhoff, R. (2017). Plant Aquaporins and CO₂. In F. Chaumont & S. D. Tyerman (Eds.), *Plant Aquaporins: From Transport to Signaling* (pp. 255-265). Cham: Springer International Publishing.
- Uehlein, N., Lovisolo, C., Siefritz, F., & Kaldenhoff, R. (2003). The tobacco aquaporin NtAQP1 is a membrane CO₂ pore with physiological functions. *Nature*, 425(6959), 734-737. doi:10.1038/nature02027
- Uehlein, N., Otto, B., Hanson, D. T., Fischer, M., McDowell, N., & Kaldenhoff, R. (2008). Function of Nicotiana tabacum aquaporins as chloroplast gas pores challenges the concept of membrane CO₂ permeability. *The Plant Cell*, 20(3), 648-657. doi:10.1105/tpc.107.054023
- von Caemmerer, S. (2000). *Biochemical models of leaf Photosynthesis*. Collingwood: CSIRO Publishing.
- von Caemmerer, S. (2021). Updating the steady state model of C₄ photosynthesis. *bioRxiv*, 2021.2003.2013.435281. doi:10.1101/2021.03.13.435281
- von Caemmerer, S., & Furbank, R. T. (1999). Modelling C₄ photosynthesis. In R. F. Sage & R. K. Monson (Eds.), *The biology of C₄ Photosynthesis* (pp. 173-211). London: Academic Press.
- von Caemmerer, S., & Furbank, R. T. (2016). Strategies for improving C₄ photosynthesis. *Current Opinion in Plant Biology*, 31, 125-134. doi:<http://dx.doi.org/10.1016/j.pbi.2016.04.003>
- von Caemmerer, S., Quinn, V., Hancock, N. C., Price, G. D., Furbank, R. T., & Ludwig, M. (2004). Carbonic anhydrase and C₄ photosynthesis: a transgenic analysis. *Plant, Cell & Environment*, 27(6), 697-703.
- Wang, C., Hu, H., Qin, X., Zeise, B., Xu, D., Rappel, W.-J., . . . Schroeder, J. I. (2016). Reconstitution of CO₂ Regulation of SLAC1 Anion Channel and Function of CO₂-Permeable PIP2;1 Aquaporin as CARBONIC ANHYDRASE4 Interactor. *The Plant Cell*, 28(2), 568-582. doi:10.1105/tpc.15.00637
- Xu, F., Wang, K., Yuan, W., Xu, W., Liu, S., Kronzucker, H. J., . . . Zhu, Y. (2019). Overexpression of rice aquaporin OsPIP1;2 improves yield by enhancing mesophyll CO₂ conductance and phloem sucrose transport. *Journal of Experimental Botany*, 70(2), 671-681. doi:10.1093/jxb/ery386
- Yang, B., Fukuda, N., van Hoek, A., Matthay, M. A., Ma, T., & Verkman, A. S. (2000). Carbon Dioxide Permeability of Aquaporin-1 Measured in Erythrocytes and Lung of Aquaporin-1 Null Mice and in Reconstituted Proteoliposomes. *Journal of Biological Chemistry*, 275(4), 2686-2692. Retrieved from <http://www.jbc.org/content/275/4/2686.abstract>
- Zelazny, E., Borst, J. W., Muylaert, M., Batoko, H., Hemminga, M. A., & Chaumont, F. (2007). FRET imaging in living maize cells reveals that plasma membrane aquaporins interact to regulate their subcellular localization. *Proceedings of the National Academy of Sciences*, 104(30), 12359. doi:10.1073/pnas.0701180104

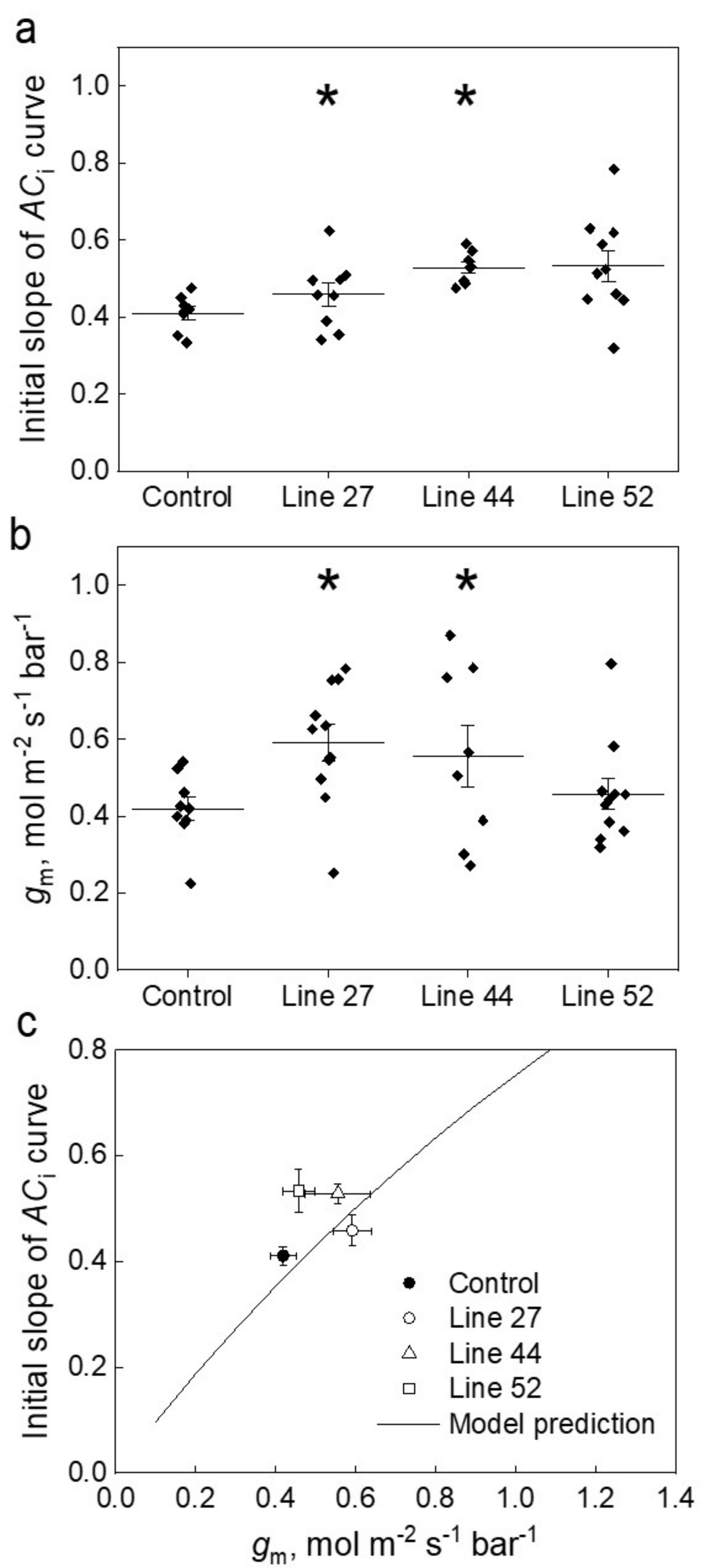
Table 1. Properties of *S. viridis* plants expressing *SiPIP2;7-FLAG* in mesophyll cells. PEPC, PEP carboxylase; Rubisco, ribulose biphosphate carboxylase oxygenase; LMA, leaf mass per area. Azygous plants of line 44 were used as control. Mean \pm SE, $n = 3$ except for biomass ($n = 8$). Three-weeks old plants before flowering were used for all analyses. No significant difference was found between the transgenic and control plants (one-way ANOVA, $\alpha = 0.05$).

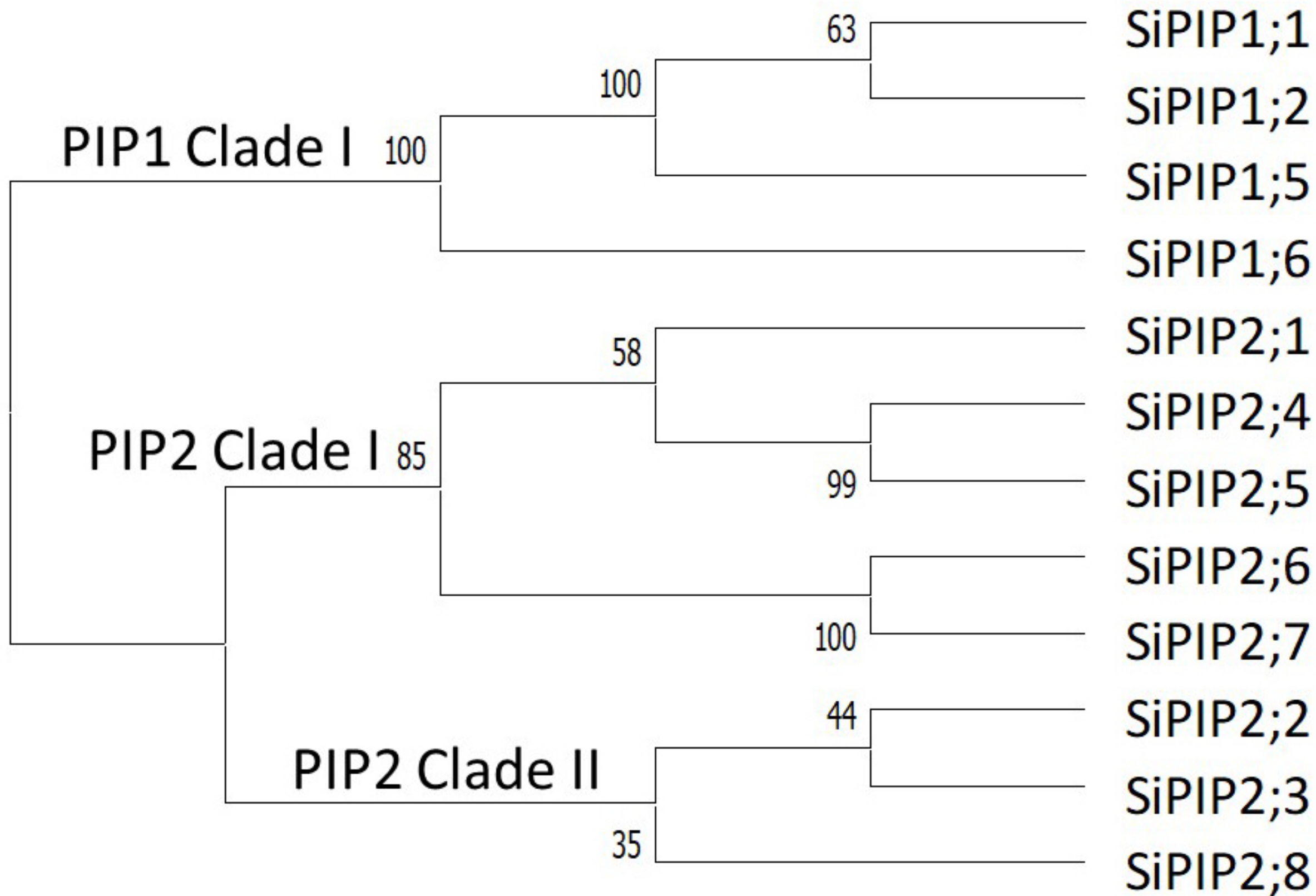
Parameter	Control	Line 27	Line 44	Line 52
PEPC activity, $\mu\text{mol CO}_2 \text{ m}^{-2} \text{ s}^{-1}$	220.1 \pm 25.8	197.6 \pm 12.7	208.7 \pm 7.9	218.5 \pm 3.5
CA hydration rate, $\text{mol m}^{-2} \text{ s}^{-1} \text{ bar}^{-1}$	6.50 \pm 0.10	6.32 \pm 0.22	5.34 \pm 0.67	5.35 \pm 0.56
Rubisco active sites, $\mu\text{mol m}^{-2}$	12.17 \pm 0.63	12.53 \pm 0.54	12.84 \pm 0.13	12.63 \pm 0.74
Chlorophyll (<i>a+b</i>), mmol m^{-2}	0.71 \pm 0.07	0.72 \pm 0.04	0.72 \pm 0.05	0.72 \pm 0.08
Chlorophyll <i>a/b</i>	5.01 \pm 0.16	5.08 \pm 0.05	4.97 \pm 0.09	5.07 \pm 0.15
LMA, g (dry weight) m^{-2}	23.6 \pm 1.6	24.0 \pm 1.5	25.6 \pm 1.3	25.4 \pm 1.3
Shoot biomass, g (dry weight) plant^{-1}	2.06 \pm 0.36	2.01 \pm 0.20	2.23 \pm 0.31	2.24 \pm 0.34
Root biomass, g (dry weight) plant^{-1}	0.27 \pm 0.07	0.28 \pm 0.03	0.34 \pm 0.06	0.35 \pm 0.05



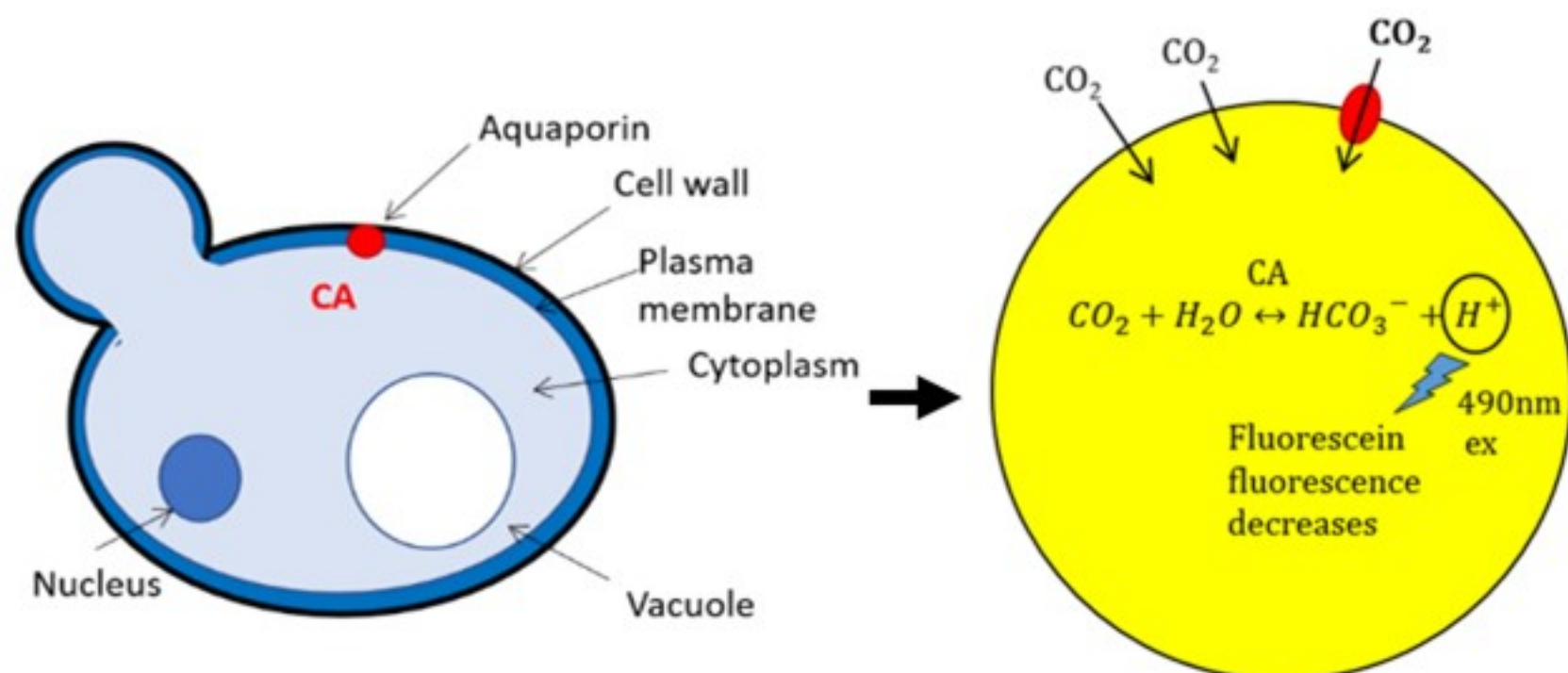
a**b****c**

a CO_2 assimilation rate, $\mu\text{mol m}^{-2} \text{s}^{-1}$ **b** ϕPSII 

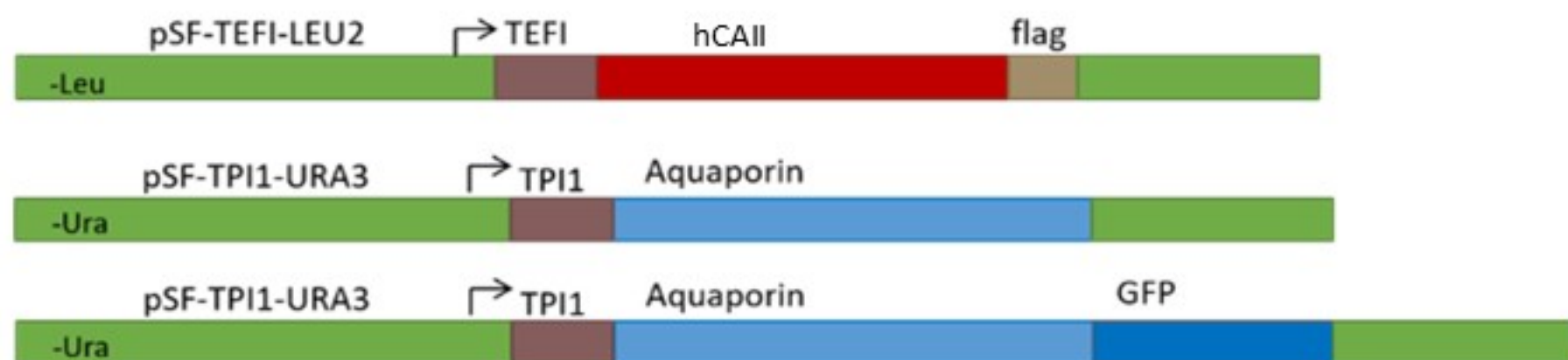




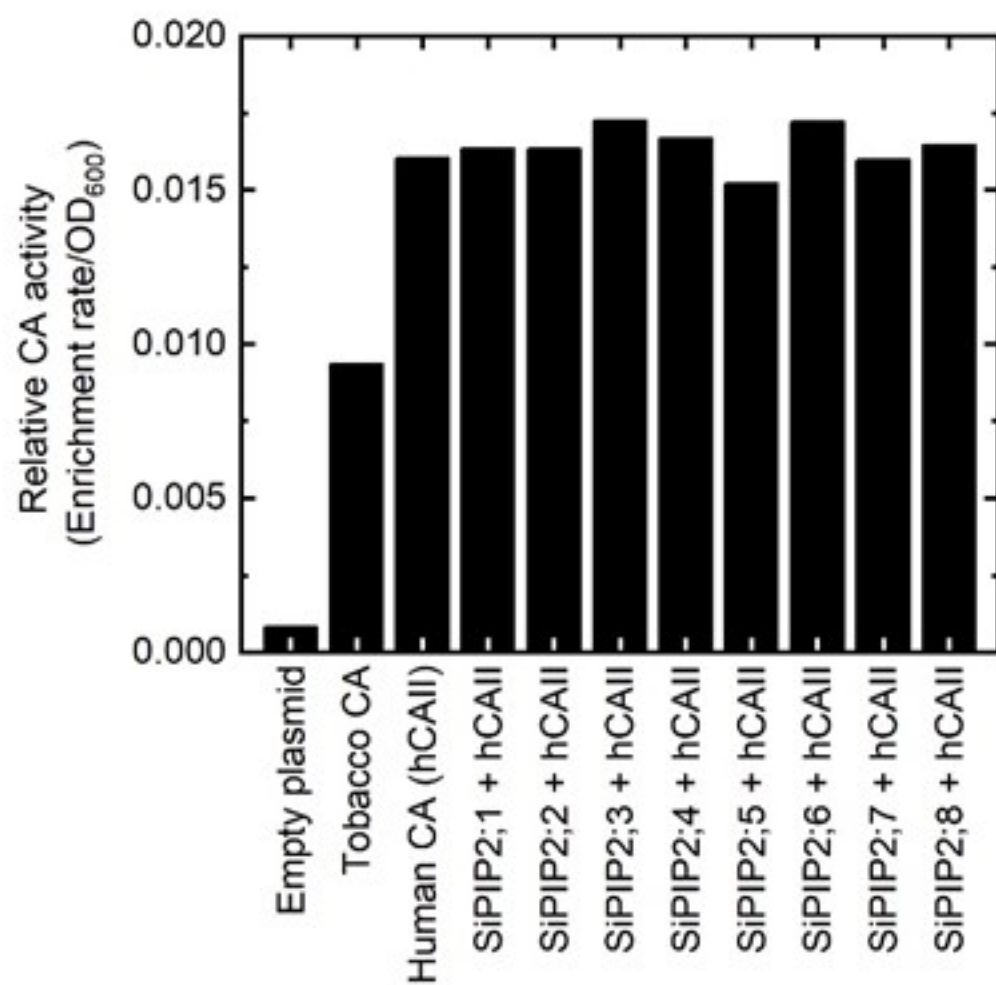
a



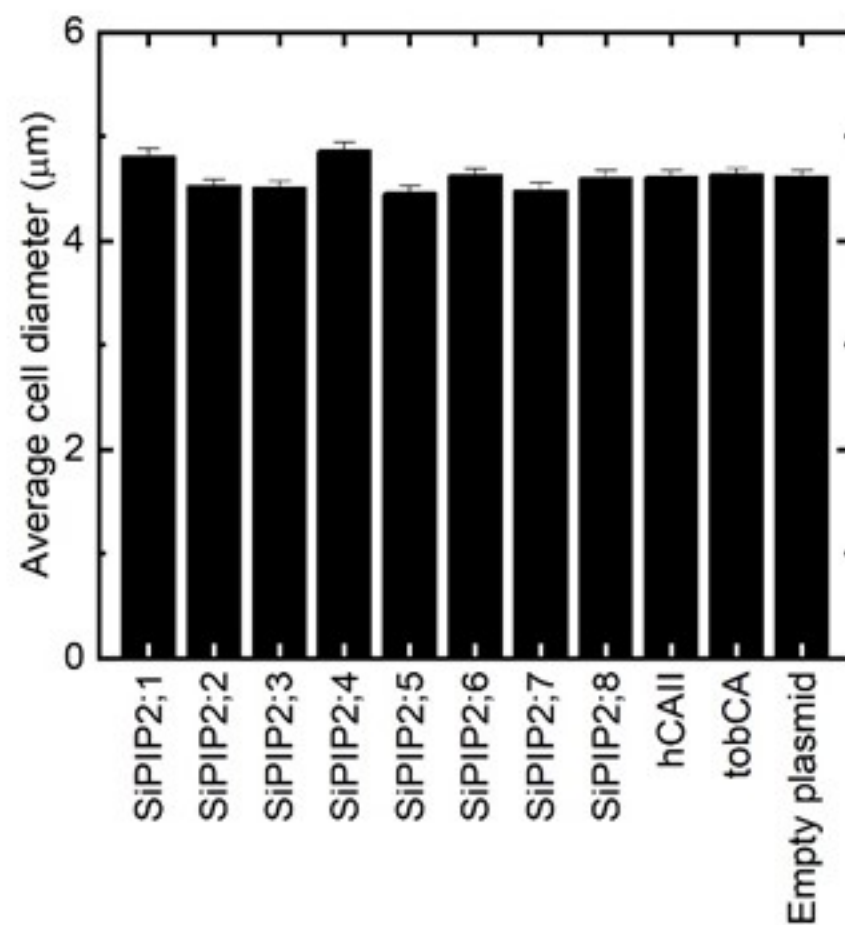
b

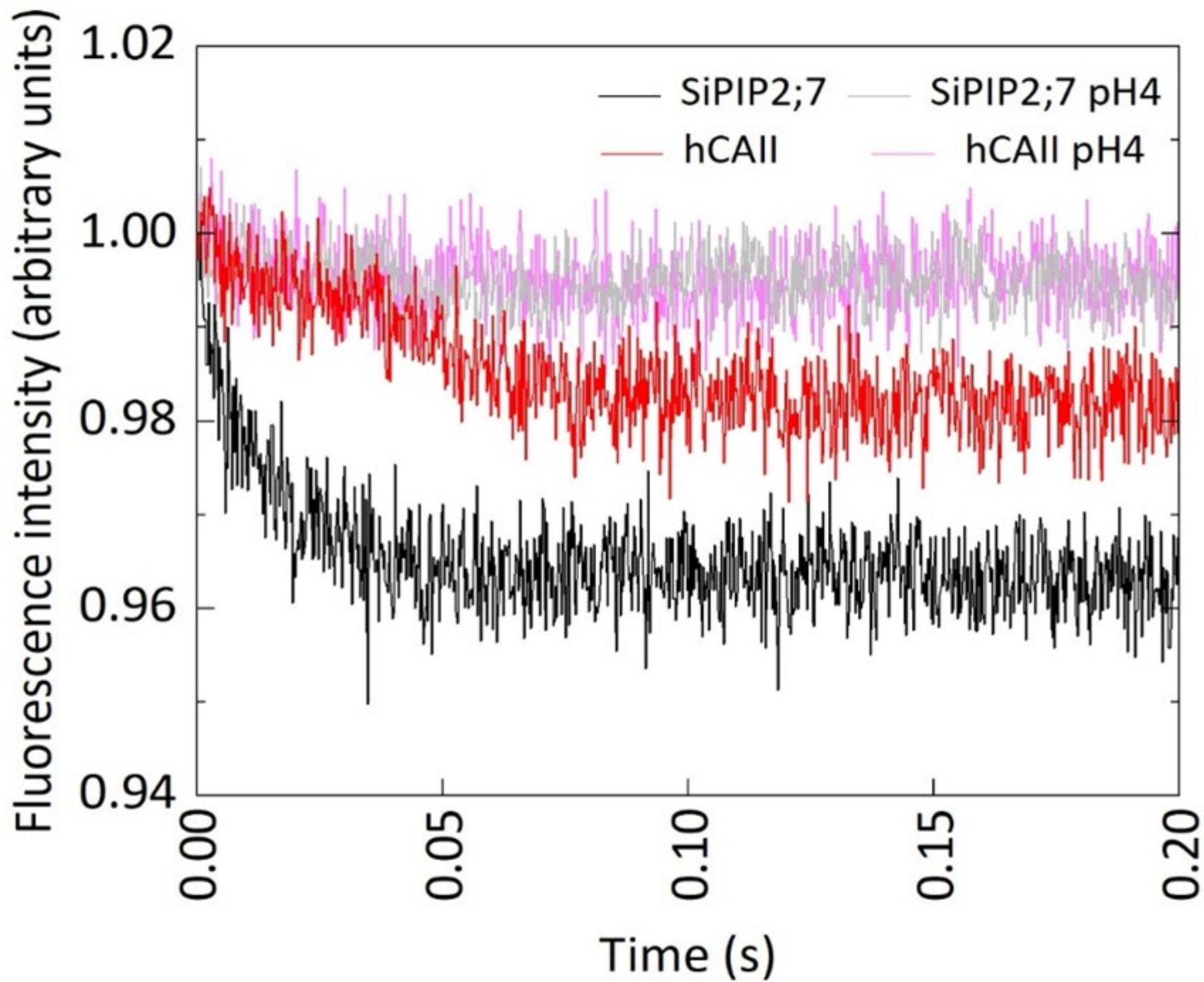


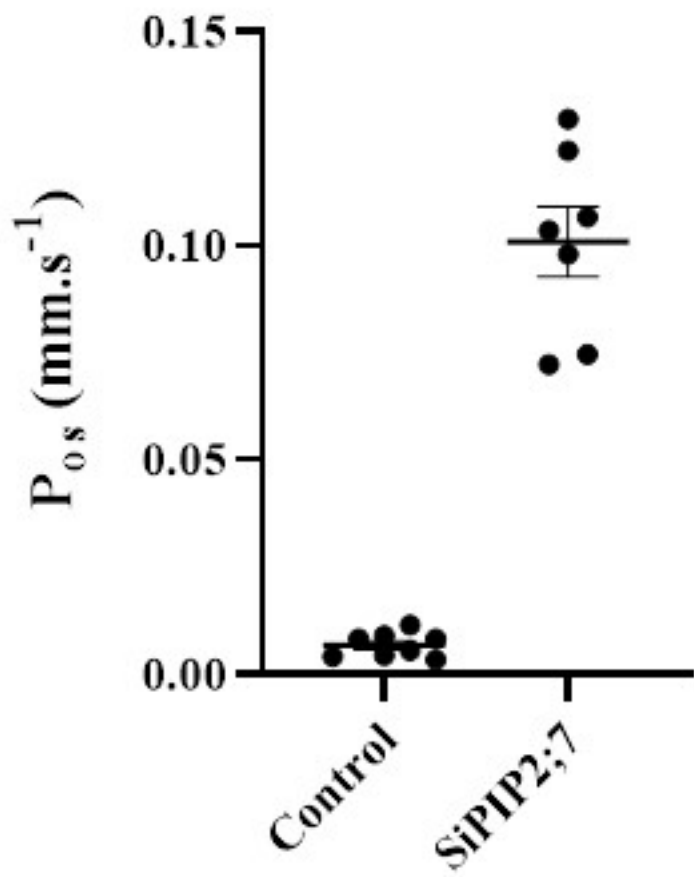
c



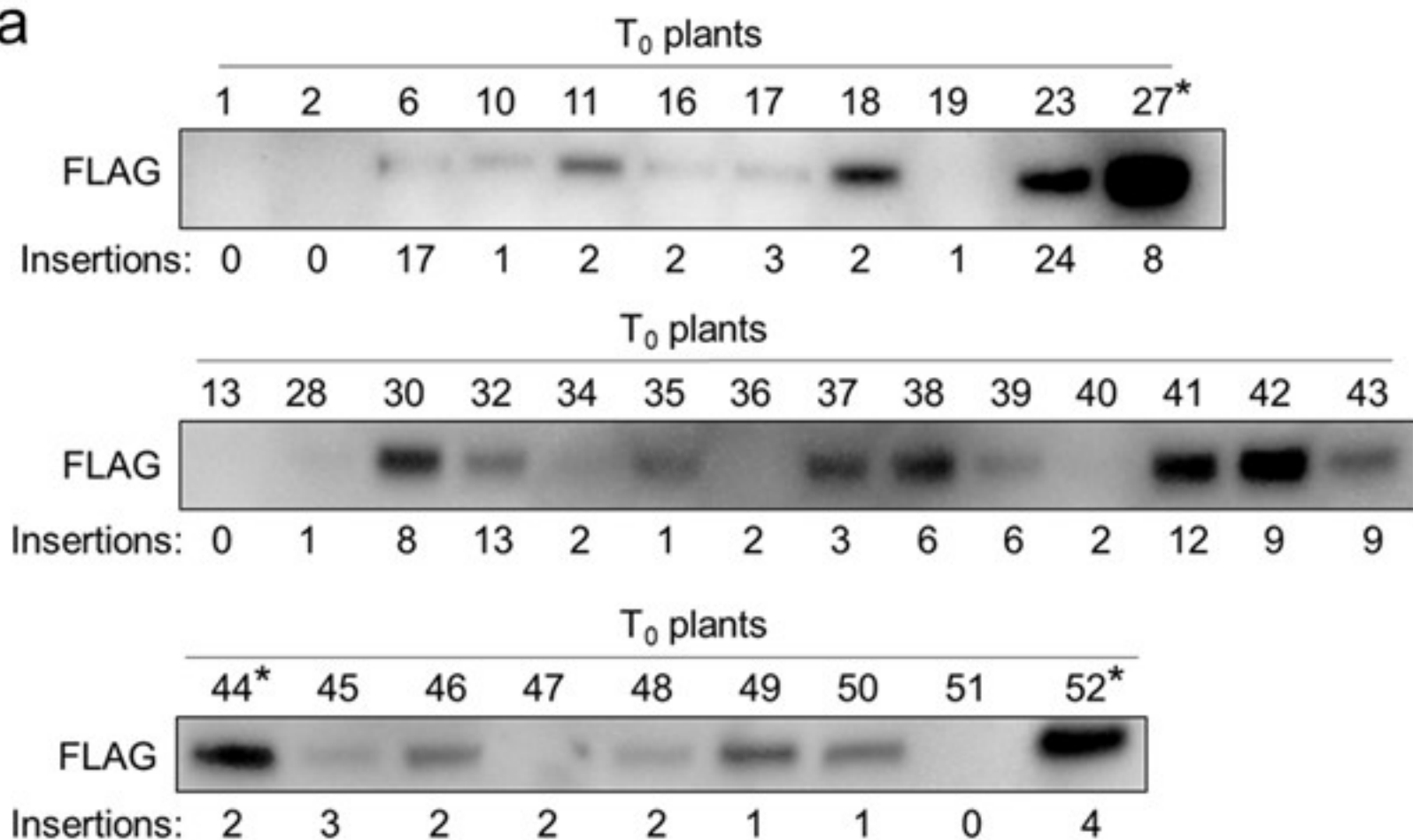
d







a



b

